ELSEVIER

Contents lists available at ScienceDirect

# Journal of Inorganic Biochemistry

journal homepage: www.elsevier.com/locate/jinorgbio





# Bridging the functional gap between reactivity and inhibition in dehaloperoxidase B from *Amphitrite ornata*: Mechanistic and structural studies with 2,4- and 2,6-dihalophenols

Talita Malewschik, Leiah M. Carey, Vesna de Serrano, Reza A. Ghiladi

Department of Chemistry, North Carolina State University, Raleigh, NC 27695-8204, United States

### ARTICLE INFO

Keywords: Catalytic globin Dihalophenol Heme Oxidation Peroxidase Peroxygenase

### ABSTRACT

The multifunctional catalytic globin dehaloperoxidase (DHP) from the marine worm Amphitrite ornata was shown to catalyze the  $\rm H_2O_2$ -dependent oxidation of 2,4- and 2,6-dihalophenols (DXP; X = F, Cl, Br). Product identification by LC-MS revealed multiple monomeric products with varying degrees of oxidation and/or dehalogenation, as well as oligomers with n up to 6. Mechanistic and  $^{18}\rm O$ -labeling studies demonstrated sequential dihalophenol oxidation via peroxidase and peroxygenase activities. Binding studies established that 2,4-DXP (X = Cl, Br) have the highest affinities of any known DHP substrate. X-ray crystallography identified different binding positions for 2,4- and 2,6-DXP substrates in the hydrophobic distal pocket of DHP. Correlation between the number of halogens and the substrate binding orientation revealed a halogen-dependent binding motif for mono- (4-halophenol), di- (2,4- and 2,6-dihalophenol) and trihalophenols (2,4,6-trihalopenol). Taken together, the findings here on dihalophenol reactivity with DHP advance our understanding of how these compounds bridge the inhibitory and oxidative functions of their mono- and trihalophenol counterparts, respectively, and provide further insight into the protein structure-function paradigm relevant to multifunctional catalytic globins in comparison to their monofunctional analogs.

# 1. Introduction

The marine worm *Amphitrite ornata* is a terebellid polychaete found in coastal mudflats [1], an environment that often contains a wide variety of organobromine compounds spanning bromophenols, bromoindoles, and bromopyrroles [2–4]. Secreted by other organisms as a chemical defense mechanism [4,5], these halometabolites are tolerated by *A. ornata* in what to-date appears to be a unique survival mechanism, namely that it utilizes its hemoglobin [6] as a chemical detoxification enzyme. Named dehaloperoxidase (DHP) and described as a catalytic globin by Lebioda [7], DHP was found to be the first oxygen-transport protein to possess a biologically relevant peroxidase activity [1,4–8].

This initially identified native enzymatic activity for DHP, discovered in 1996, was for the oxidative dehalogenation of 2,4,6-trihalophenols (2,4,6-TXP; X = F, Cl, Br) into their corresponding 2,6-dihalo-1,4-benzo-quinones, a reaction that was found to proceed through a peroxidase mechanism [5,8–25]. Mechanistic investigations revealed that 2,4,6-TXP oxidation occurs via two sequential one-electron steps initiated upon  $H_2O_2$  binding, consistent with a traditional mechanism [8,9,18,20,26,27] that utilizes ferryl intermediates Compound I [(Por $\bullet$ +)  $Fe^{IV}$ =O AA] [11] and Compound II [(Por)  $Fe^{IV}$ =O AA] [12] as the catalytic species responsible for substrate oxidation. Multiple TXP binding sites have been suggested by NMR [18,28–31], resonance Raman [18,20,32–36], and magnetic circular dichroism [23,37]

Abbreviations: 4-BP, 4-bromophenol; 4-CP, 4-chlorophenol; 2,4-DFP, 2,4-difluorophenol; 2,4-DCP, 2,4-dichlorophenol; 2,4-DBP, 2,4-dibromophenol; 2,6-DFP, 2,6-difluorophenol; 2,6-DCP, 2,6-dichlorophenol; 2,6-DBP, 2,6-dibromophenol; 2,4,6-TCP, 2,4,6-trichlorophenol; 2,4,6-TBP, 2,4,6-tribromophenol; 4-Br-C, 4-bromo-ocresol; 4-NC, 4-nitrocatechol; 4-NP, 4-nitrophenol; Compound I, two-electron oxidized heme cofactor compared to the ferric form commonly referred to as iron(IV)-oxo porphyrin π-cation radical [Por\*+ Fe<sup>IV</sup>=O]; Compound II, one-electron oxidized heme cofactor when compared to the ferric form [Por Fe<sup>IV</sup>=O or Por Fe<sup>IV</sup>-OH]; Compound ES, two-electron-oxidized state containing both a ferryl center and a tyrosyl radical initially located on Tyr38, analogous to Compound ES in cytochrome c peroxidase [(Por)Fe(IV) = O \*Tyr38]; DHP, dehaloperoxidase; DMPO, 5,5-dimethyl-1-pyrroline N-oxide; DMSO, dimethyl sulfoxide; HRP, horseradish peroxidase; HSM, horse skeletal muscle myoglobin; ESI, electrospray ionization; SFX, serial femtosecond crystallography; TFA, trifluoroacetic acid; WT, wild-type..

E-mail address: Reza\_Ghiladi@ncsu.edu (R.A. Ghiladi).

<sup>\*</sup> Corresponding author.

spectroscopic studies' which together revealed a dependence between halogen size and substrate binding affinity. X-ray crystallographic methods have elucidated binding sites for 2,4,6-TBP [38] and 2,4,6-TCP [24,39], showing that both molecules bind in the distal pocket, where 2,4,6-TBP binds internally in the Xe1 binding pocket and 2,4,6-TCP has two orientations, internal (in the Xe1 hydrophobic pocket) and external towards the heme edge, in an orientation that could still facilitate heme activation and subsequent reactivity.

In more recent years, DHP has also been shown to catalyze substrate oxidation through peroxygenase [40-42], oxidase [40], and oxygenase [43] activities in addition to its physiological O2-transport function, establishing DHP as a multifunctional catalytic globin with four oxidative functions all occurring at a single heme active site. Accordingly, the active site of DHP can accommodate a wide variety of aromatic compounds, including substituted indoles [40,44], pyrroles [45], phenols (halophenols, guaiacols, cresols) [23,42,44,46], as well as compounds from the azole family [47]. In the case of phenolic substrates, a number of outcomes have been observed: peroxidase activity in the oxidation of 2,4,6-trihalophenol [9,20,24,25] and methoxyphenol (guaiacol) [46], sequential peroxygenase and peroxidase activities in the oxidation of 4nitrophenol [41], sequential peroxygenase and oxidase activities in the oxidation of 5-Br-indole, and simultaneous peroxidase and peroxygenase activities in the oxidation of methylphenol (cresol) [42]. While substrate conversion of 4-halophenols (4-XP) has been previously observed [5], they mainly function as inhibitors of DHP in the presence of other substrates [30,32,35,36,48]. X-ray crystallographic studies have elucidated the 4-XP (X = F, Cl, Br and I) [35,39,49] binding site within the distal pocket directly over the heme cofactor, residing between the Fe and heme  $\gamma$  edge. Mutagenic studies [32,50,51] and molecular dynamic simulations [52] have demonstrated that 4-XP binding stabilization depends upon distal pocket polarity, H-bonding contributions of active site residues, and hydrophobic stabilization of the halide atom. Given its position above the heme cofactor, the 4-XP binding site has implications towards its mechanistic role due to its orientation in a position that can hinder catalytic activation by: i) excluding other ligands from entering the pocket, ii) sterically preventing H2O2 from binding to the heme-Fe, iii) forcing the catalytically important distal histidine (H55) out of the pocket into the 'open' conformation [25,35,49,53,54], thus preventing its participation in heterolytic cleavage of the peroxide O-O bond required for heme activation, and iv) providing an alternative site of oxidation that outcompetes other substrates.

Our extensive mechanistic understanding of DHP chemistry with 4-XP (inhibitor of both peroxidase and peroxygenase DHP activities) and 2,4,6-TXP (peroxidase substrate) only serves to highlight a clear knowledge gap as it pertains to the reactivity of DHP with dihalophenols (DXP). While 2,4-DXP and 2,6-DXP (X = Br and Cl) were shown many years ago to be DHP substrates [5], no mechanistic studies have been performed to-date, and it remains unknown which of the four enzymatic activities of DHP catalyzes their oxidation, nor what the products are. While recent crystallographic studies performed by serial femtosecond X-ray crystallography (SFX) for DHP isoenzyme B [55,56] complexed with 2,4-DCP have provided valuable structural information [44], a more thorough investigation of DXP reactivity with DHP (and its mechanistic implications) is needed to understand how these compounds bridge the inhibitory and oxidative functions of their mono- and trihalophenol counterparts, respectively. To that end, here we explored the reactivity of 2,4- and 2,6-dihalophenols (2,4-DXP and 2,6-DXP, where X = F, Cl, Br) with DHP B using biochemical assays and isotopic labeling studies paired with spectroscopic and structural methods. As will be shown, our results demonstrate that DHP unexpectedly oxidizes DXP substrates via sequential peroxidase and peroxygenase activities, findings that will provide further insights into the protein structure-function paradigm as it pertains to multifunctional catalytic globins in comparison to their monofunctional counterparts.

### 2. Experimental

### 2.1. Materials and methods

Isotopically labeled  $\mathrm{H}_{2}^{18}\mathrm{O}_{2}$  (90%  $^{18}\mathrm{O}\text{-enriched})$  and  $\mathrm{H}_{2}^{18}\mathrm{O}$  (98%  $^{18}\mathrm{O}\text{-}$ enriched) were purchased from Icon Isotopes (Summit, NJ). Acetonitrile (ACN) and trifluoroacetic acid (TFA) were HPLC grade, and all other chemicals were purchased from VWR, Sigma-Aldrich or Fisher Scientific and used without further purification. Ferric WT DHP B was expressed and purified according to the procedure in the Supporting Information by modifying previously reported methods [13,20,21,41]. Oxyferrous DHP was obtained by the aerobic addition of excess ascorbic acid, followed by desalting (PD-10/Sephadex G-25). Horse skeletal muscle (HSM) myoglobin ( $\varepsilon_{soret}=188,000~\text{M}^{-1}~\text{cm}^{-1}$ ) [57] and horseradish peroxidase (HRP) ( $\varepsilon_{\text{soret}} = 102,000 \text{ M}^{-1} \text{ cm}^{-1}$ ) [58] were purchased from Sigma-Aldrich and used as received. Stock solutions of i) substrates were prepared in MeOH (10 mM) and stored in the dark at -80 °C until needed, ii) aqueous solutions of concentrated potassium cyanide (KCN), used as a quencher, were stored at 4 °C, and iii) solutions of H<sub>2</sub>O<sub>2</sub> (reaction pH) were prepared fresh daily, the concentration determined spectrophotometrically ( $\varepsilon_{240 \text{ nm}} = 43.6 \text{ M}^{-1} \text{ cm}^{-1}$ ) [59], and kept on ice until needed.

### 2.2. Enzyme assay protocol

Reactions were performed in triplicate in 100 mM KP<sub>i</sub> (pH 7, unless otherwise indicated) with 5% MeOH at 25  $^{\circ}$ C (final volume 250  $\mu$ L). Ferric DHP B (10  $\mu$ M) and substrate (500  $\mu$ M) were mixed first, and the reaction was initiated upon addition of H<sub>2</sub>O<sub>2</sub> (500 µM). After 5 min, reactions were quenched with excess KCN. The reaction was diluted 4fold with 600 µL of 100 mM KP<sub>i</sub> (reaction pH). Diluted samples were analyzed using a Waters e2695 Bioseparations Module coupled with a Waters 2998 Photodiode Array Detector and equipped with a Thermo-Scientific ODS Hypersil (150  $\times$  4.6 mm) 5  $\mu m$  particle size  $C_{18}$  column. Separation of observed analytes was performed using a linear gradient of binary solvents (solvent A - H2O containing 0.1% trifluoroacetic acid (TFA); solvent B - ACN containing 0.1% TFA). Elution was performed at a flow rate of 1.5 mL/min with the following conditions: 95:5 (A:B) to 5:95 using a linear gradient over 11 min; 5:95 isocratic for 3 min; 5:95 to 95:5 using a linear gradient over 1 min, and then isocratic for 9 min. Data analysis was performed using the Empower 3 software package (Waters Corp.). Mechanistic probes were also employed: 500 μM 4-bromophenol (MeOH), 500 μM D-mannitol (KP<sub>i</sub>), 100 mM 5,5-dimethyl-1-pyrroline N-oxide (DMPO; MeOH) or 10% ν/ν DMSO, and adjustments were made to ensure a final 5% MeOH concentration for all reactions except DMPO (10% MeOH final). Control experiments were also performed as above, either in the absence of hydrogen peroxide (non-oxidant control) or the absence of enzyme (non-enzymatic control).

# 2.3. LC-MS studies

For product identification, experiments were analyzed by LC-MS using a Thermo Fisher Scientific Exactive Plus Orbitrap mass spectrometer with heated-electrospray ionization (HESI) probe (Thermo Scientific, San Jose, CA) equipped with a Thermo Hypersil Gold (50  $\times$  2.1 mm) 1.9  $\mu m$  particle size  $C_8$  column. Analyte separation was performed using a linear gradient of binary solvents (solvent A -  $H_2O$  containing 0.1% formic acid: solvent B - ACN), with an elution profile (0.5 mL/min, A:B) of 99:1 to 0:100 over 20 min. Samples were analyzed using electrospray ionization in negative mode to provide observation of the [M-H] $^-$  species. Spectra were collected while scanning in the range from 100 to 1500 m/z. Data analysis was performed using Thermo Xcalibur software. Reactions [5 mM KP<sub>1</sub>, (pH 7), 5% MeOH ( $\nu/\nu$ ); 250  $\mu$ L final volume] containing 10  $\mu$ M enzyme and 500  $\mu$ M of substrate were initiated by addition of 500  $\mu$ M of H<sub>2</sub>O<sub>2</sub>, quenched with excess KCN after

5 min, and the undiluted reaction mixture analyzed (20  $\mu$ L injection aliquots). For the <sup>18</sup>O labeling studies, the reactions were carried out in the same manner, but under three different conditions: i)  $H_2^{18}O/H_2O_2$ , ii)  $H_2O/H_2^{18}O_2$ , and iii)  $H_2^{18}O/H_2^{18}O_2$ , where buffer was replaced with  $H_2^{18}O$ , and/or the  $H_2O_2$  was replaced with labeled  $H_2^{18}O_2$  to ensure >90% of labeled <sup>18</sup>O was present.

# 2.4. Binding studies

Adapted from previously published protocols [60]' 2,4- and 2,6-DXP stock solutions were prepared in MeOH. The UV–visible spectrophotometer was referenced using a solution of 10  $\mu M$  ferric WT DHP B in 100 mM KP $_{\rm i}$  (pH 7) containing 5% MeOH. Difference spectra were acquired in triplicate in the presence of 0.21–750 equiv. substrate while maintaining both enzyme and MeOH concentrations constant. Analysis by nonlinear regression was performed using the GraFit software package (Erithacus Software Ltd.).

# 2.5. Protein crystallization and X-ray diffraction studies

Non-His tagged DHP B was overexpressed and purified per literature protocol [41]. Crystals were obtained through the hanging-drop vapor diffusion method. DHP B was concentrated to 12 mg/mL in 20 mM sodium cacodylate buffer (pH 6.4) and crystals were grown from mother liquor solutions of 28-32% PEG 4000 and 0.2 M ammonium sulfate equilibrated against identical reservoir solutions. Protein-to-mother liquor ratios varied between 1:1, 1.33:1, 1.66:1 and 2:1. At 4 °C, crystals grew after 3 days and were then soaked for 12 h in substratesupplemented mother liquid and reservoir solutions of 32 or 34% PEG 4000 and 0.2 M ammonium sulfate. Substrate final concentrations of 26.5 mM 2,4-DCP (5% MeOH v/v), 36 mM 2,4-DCP (5% DMSO v/v), ~40 mM (saturated) 2,4-DBP (5% DMSO v/v), 77.4 mM 4-CP (5% DMSO v/v) and 27 mM 4-BP (5% DMSO v/v) were used to obtain the ligand bound structures 2,4-DCP, 2,4-DCP, 2,4-DBP, 4-CP and 4-BP, respectively. The 2,6-DXP substrates (X = F, Cl, Br) complexed with DHP were prepared by soaking crystals overnight at 4° C in crystallization solution supplemented with the substrate (100 mM) with a final concentration of 5% DMSO. These crystals were obtained by using MPEG 2000 as a precipitant, while the rest of the components of the reservoir solutions remained the same as above. All of the obtained crystals were cryo-protected by briefly dipping them in reservoir solution enhanced with 20% glycerol and then flash frozen in liquid N<sub>2</sub>. Data were collected at 100 K on the SER-CAT 22-ID (2,4-DCP, 4-BP and 2,6-DXP) and SER-CAT 22-BM (4-CP, 2,4-DCP and 2,4-DBP) beamlines at the APS synchrotron facility utilizing a wavelength of 1.00 Å. All data were scaled and integrated using HKL2000 [61], molecular replacement was performed with Phaser-MR [62] from the PHENIX [63] suite of programs using 3IXF [64] monomer as the search model, model building and manual placement of waters utilized COOT [65], and refinement was carried out using phenix.refine [66] from the Phenix suite of programs and Refmac5 [67] from CCP4 suite of programs [68]. X-ray crystallographic data collection and refinement statistics can be found in Tables S3 and S6.

# 2.6. Stopped-flow UV-visible spectroscopic studies

Optical spectra were recorded at room temperature using a Bio-Logic SFM-400 triple-mixing stopped flow instrument coupled to a rapid scanning diode array UV–visible spectrophotometer. Stock solutions of the substrates (10 mM) were prepared in MeOH, and all remaining solutions prepared in 100 mM KP<sub>i</sub> (pH 7). Data were collected (900 scans total) over a three-time domain regime (1.5, 15, and 150 ms; 300 scans each) using the Bio Kinet32 software package (Bio-Logic). All data were evaluated using the Specfit Global Analysis System software package (Spectrum Software Associates) and fit to exponential functions as one-step/two-species or two-step/three-species irreversible mechanisms

where applicable. For data that did not properly fit these models, experimentally obtained spectra at selected time points detailed in the figure legends are shown. Data were baseline corrected using the Specfit function.

The protein and H<sub>2</sub>O<sub>2</sub> solutions with appropriate concentrations were prepared in 100 mM KPi (pH 7), and the substrate solutions were made in buffer containing 5% or 10% MeOH and kept on ice until needed. Double-mixing experiments were performed as previously reported [42], by using an aging line prior to the second mixing step to observe Compound I/ES/II reactivity with 5 equiv. (2,4-DXP) and 10 equiv. (2,6-DXP), as follows: (i) Compound I was pre-formed from the reaction of ferric DHP B (Y28F/Y38F) [11] with 10 equiv. H2O2 in an aging line for 75 ms prior to mixing with the substrate; (ii) Compound ES was pre-formed by reaction of ferric WT DHP B with 10 equiv. of H<sub>2</sub>O<sub>2</sub> in an aging line for 420 ms prior to mixing with the substrate [13,20]; and (iii) Compound II was pre-formed from oxyferrous DHP B that was preincubated with 1 equiv. 2,4,6-TCP and then reacted with 10 equiv. of  $H_2O_2$  in an aging line for 3.2 s prior to mixing with the substrate [12,46]. In addition, oxyferrous reactivity was probed using single-mixing methods by reacting 10 µM oxyferrous DHP B pre-incubated with 5 equiv. (2,4-DXP) or 10 equiv. (2,6-DXP) with 10 equiv. H<sub>2</sub>O<sub>2</sub> in a 1:1

# 3. Results

# 3.1. Substrate reactivity assays

The reactivity of the selected substrates was investigated in enzymatic assays using  $H_2O_2$  as the oxidant in the presence of DHP B at pH 7, and the results were monitored by HPLC. Reactions were initiated upon addition of 500  $\mu M$   $H_2O_2$  to a solution containing a preincubated mixture of 10  $\mu$ M enzyme and 500  $\mu$ M substrate, and the reaction was quenched after 5 min with an excess of KCN. The reported percent conversion was determined by monitoring the loss of the substrate peak (Table 1). Representative HPLC chromatograms of the reactions as well as the characteristic UV-visible spectrum for each substrate are shown in Fig. 1 and Fig. S1. At pH 7, all substrates showed reactivity and the percent conversion ranged from 52% to 96% (26 to 48 turnovers) for 2,4-DBP and 2,6-DBP, respectively. Multiple product peaks were observed in the chromatogram of all substrates and identification of the products was determined via LC-MS (vide infra). In the case of 2,4-DXP, an inverse relationship was observed between the halogen size and the percent conversion (F > Cl  $\sim$  Br), with an almost 2-fold difference between the highest and lowest conversion. Similar results were observed when DHP catalyzed the oxidation of 4-X-o-cresols [42], and the opposite trend was observed for the oxidation of 5-X-indoles [40]. For the 2,6-DXP series, all three substrates showed high percent conversions (around 96%) and no noticeable trend was observed in terms of halogen size, which is similar to what was observed for the oxidation of 4-X-oguaiacols [46]. No reactivity was observed in the absence of H2O2 and DHP (non-oxidant and non-enzymatic controls, respectively). In

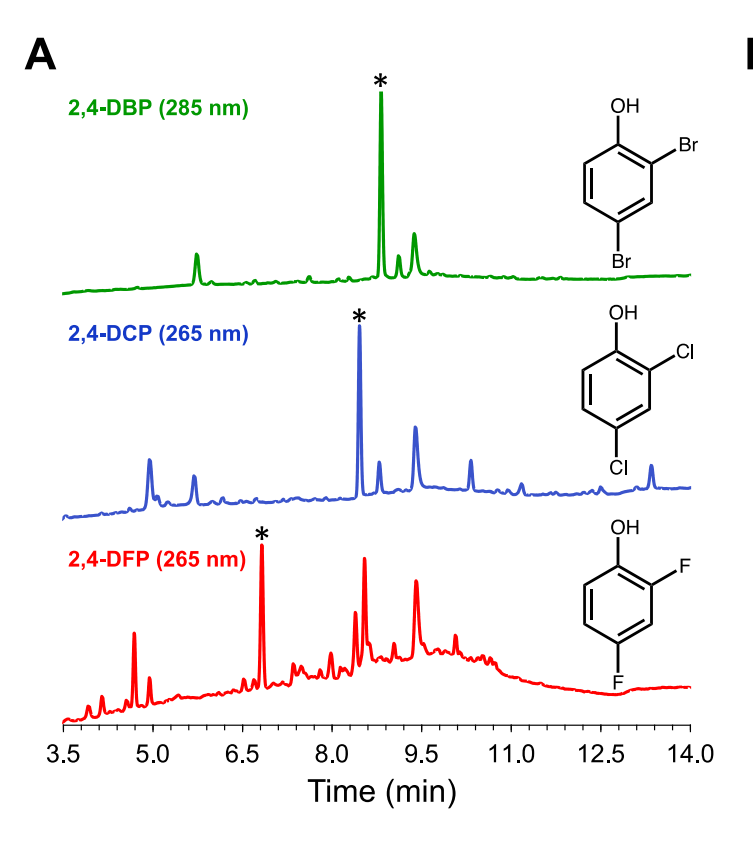
 Table 1

 Percent conversion (substrate loss) for the oxidation of 2,4- and 2,6-dihalophenols.

Ferric DHP B	Percent conversion (%)	
	Standard reaction	+DMPO <sup>a</sup>
2,4-difluorophenol (2,4-DFP)	90.4 (± 3.1)	84.9 (± 5.2)
2,4-dichlorophenol (2,4-DCP)	$61.3~(\pm~4.1)$	$50.6~(\pm~1.3)$
2,4-dibromophenol (2,4-DBP)	49.9 (± 4.4)	$34.9 (\pm 2.6)$
2,6-difluorophenol (2,6-DFP)	95.7 ( $\pm$ 1.2)	$85.7~(\pm~2.5)$
2,6-dichlorophenol (2,6-DCP)	95.4 (± 1.9)	77.9 ( $\pm$ 0.7)
2,6-dibromophenol (2,6-DBP)	96.2 ( $\pm$ 2.0)	84.8 ( $\pm$ 3.2)

Reaction conditions. [enzyme] = 10  $\mu M,$  [substrate] = [H $_2O_2]$  = 500  $\mu M,$  100 mM KP $_i$  (pH 7), 5% MeOH, 5 min.

<sup>&</sup>lt;sup>a</sup> Reactions performed with 10% MeOH.



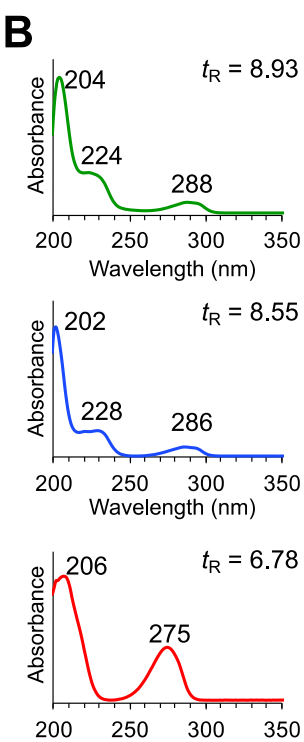


Fig. 1. (A) Representative HPLC chromatograms for the reaction of ferric WT DHP B with H<sub>2</sub>O<sub>2</sub> in the presence of 2,4-difluorophenol (red,  $\lambda = 265$  nm), 2,4-dichlorophenol (blue,  $\lambda = 265$  nm) and 2,4-dibromophenol (green,  $\lambda =$ 285 nm). (B) Respective UV-visible spectra for each substrate extracted from the chromatograms in panel A. Reaction conditions: [enzyme] = 10  $\mu M$ , [substrate] = [H<sub>2</sub>O<sub>2</sub>] = 500  $\mu M$ , 100 mM KPi, pH 7, 5% MeOH, 5 min reaction time, quenched with excess KCN. Asterisks (\*) represent the substrate peaks. (For interpretation of the references to colour in this figure legend, the reader is referred to the web version of this article.)

addition, time dependent studies were performed for all substrates, varying the time from 0.25 to 30 min (Fig. S2). Complete conversion was observed after 5–10 min for the 2,6-DXP series and after 10 min for 2,4-DCP. The conversion of 2,4-DFP ( $\sim$ 90%) remained unchanged in the time frames studied. In the case of 2,4-DBP, after 30 min only a 60% conversion was observed.

Mechanistic studies were performed to further assess the reactivity of these compounds, where 2,4-DBP and 2,6-DBP (lowest and highest percent conversion, respectively) were chosen as the two representative

**Table 2**Mechanistic investigations (enzymatic variations, pH, and radical scavengers) with 2,4- and 2,6-dibromophenol as representatives of the 2,4- and 2,6-DXP series.

	2,4-dibromophenol	2,6-dibromophenol
Enzyme variations		
Ferric DHP B	49.9 (± 4.4)	$96.2~(\pm~2.0)$
Oxyferrous DHP B	47.7 (± 2.3)	$92.1~(\pm~0.8)$
DHP A	$34.2~(\pm~5.2)$	$91.3~(\pm~0.6)$
DHP B (Y28F/Y38F)	$66.3~(\pm~9.3)$	99.7 ( $\pm$ 0.05)
HSM Mb	19.8 ( $\pm$ 1.4)	$21.2~(\pm~1.1)$
HRP	97.8 ( $\pm$ 0.9)	99.7 ( $\pm$ 0.5)
$H_2O_2$	n.d.	n.d.
enzyme	n.d.	n.d.
pH studies		
pH 5	$28.2~(\pm~0.6)$	$32.9~(\pm~0.4)$
рН 6	$34.5~(\pm~0.6)$	$61.9~(\pm~0.4)$
pH 7	49.9 (± 4.4)	$96.2~(\pm~2.0)$
pH 8	$50.0~(\pm~1.5)$	77.4 ( $\pm$ 2.0)
Mechanistic Probes		
4-bromophenol	$45.1~(\pm~2.8)$	56.6 ( $\pm$ 1.0)
DMPO <sup>a</sup>	$34.9 (\pm 2.6)$	$84.8~(\pm~3.2)$
D-mannitol	$38.3~(\pm~0.6)$	$90.4~(\pm~0.5)$
10% DMSO	44.9 (± 5.9)	94.2 ( $\pm$ 1.5)

Reaction conditions. [enzyme] =  $10 \mu M$ , [substrate] =  $[H_2O_2] = 500 \mu M$ ,  $100 mM KP_i$  (pH 7), 5% MeOH, 5 min; n.d. = no reactivity detected.

substrates (Table 2).

# 3.1.1. Enzyme variations

Wavelength (nm)

The reactivity of the two brominated substrates was investigated by employing oxyferrous DHP B (hemoglobin-active state). The percent conversion was unaffected (within error) compared to ferric DHP B, which indicates that substrate oxidation can be initiated from either the peroxidase-active (Fe<sup>II</sup>) or hemoglobin-active (Fe<sup>II</sup>-O<sub>2</sub>) states, a result that has been observed before for DHP-dependent oxidation reactions [9,17,12,40-42,46]. DHP isoenzyme A [55] exhibited attenuated activity for both 2,4- and 2,6-DBP, a result that has been previously noted for the oxidation of 2,4,6-trihalophenols [20], indoles [40], and nitrophenols [41]. Reactions with the DHP B(Y28F/Y38F) mutant that yields Compound I showed an increase in reactivity for both substrates, a result that has been observed before in the oxidation of 2,4,6-TCP [11]. As expected, the canonical peroxidase HRP showed complete conversion for both substrates, in line with previous studies with 4-Br-o-cresol (4-Br-C) [42], whereas HSM myoglobin showed attenuated conversion compared to WT DHP, similar to its observed reactivity with 4-Br-C and 4-/5-Br-o-guaiacol substrates [46]. No significant differences in product distribution were noted for any of the aforementioned reactions (data not shown).

# 3.1.2. pH studies

A pH-dependence was noted for the oxidation of both substrates, with ~2-fold (2,4-DBP) and ~3-fold (2,6-DBP) increases in percent conversion when the reaction pH increased from 5 to 8 (Table 2). At pH 8, a slight decrease in substrate loss was observed for 2,6-DBP (p $K_a$  6.7) compared to pH 7, while 2,4-DBP (p $K_a$  7.8) was virtually unchanged between these two values [69]. Similar results were observed in the DHP-catalyzed oxidation of 4-Br-C, however the reaction showed higher conversion in pH 8–9, which was attributed to the fact that the p $K_a$  of the acid-alkali transition of DHP is at 8.1 [19,42]. No significant change in product distribution was observed as a function of pH (data not shown). Given these results, we established that the optimal pH for the oxidation

<sup>&</sup>lt;sup>a</sup> Reactions performed with 10% MeOH.

of both substrates was 7.

# 3.1.3. Radical scavengers

The presence of radical scavengers such as DMPO, D-mannitol or DMSO only slightly decreased (5–10%) the percent of substrate conversion, suggesting that freely-diffusible radicals are not playing a role in the oxidation of either the 2,4- or 2,6-DBP substrates, a finding that has literature precedent for DHP in the oxidation of guaiacols [46], and cresols [42]. While no significant change in the product distribution was observed in the presence of D-mannitol or DMSO (data not shown), a small change in the product distribution for the reactions performed in the presence of DMPO was found.

### 3.1.4. Inhibitor

Additionally, the reactivity of both 2,4- and 2,6-DBP substrates was investigated in the presence of 4-bromophenol (4-BP), a known DHP peroxidase and peroxygenase inhibitor ( $K_{\rm d}=305~\mu{\rm M},~K_{\rm i}=0.15\pm0.03~{\rm mM}$ ) [36,48]. The percent conversion of 2,4-DBP (45.1%) was unaffected (within error) by the presence of 4-BP, which can be explained by the high affinity of DHP for this substrate ( $K_{\rm d}=6.4~\mu{\rm M},~{\rm vide}~{\rm infra}$ ) compared to 4-BP. On the other hand, a decrease in DHP reactivity with 2,6-DBP was noted when 4-BP was present, consistent with the weaker binding of 2,6-DBP ( $K_{\rm d}\sim7000~\mu{\rm M}$ ) compared to 4-BP. No significant change in product distribution was observed in the presence of 4-BP (data not shown).

# 3.2. Identification of reaction products by LC-MS

It is clear from the results of the enzymatic assays presented above that the substrates in the scope of this study, 2,4-DXP and 2,6-DXP (X = F, Cl, Br), underwent a DHP-catalyzed oxidation in the presence of  $\rm H_2O_2$  under physiological conditions. As these substrates provide a connection between the inhibitory activity of 4-halophenols (4-XP) and the peroxidase activity of 2,4,6-trihalophenols (2,4,6-TXP), product identification studies were conducted to provide evidence of oxidation via either peroxidase or peroxygenase mechanisms.

The H<sub>2</sub>O<sub>2</sub>-dependent oxidation of 2,4- and 2,6-dihalophenols as catalyzed by ferric WT DHP B (5 mM KP  $_{\!i},$  pH 7, 5% MeOH) was analyzed by LC-MS (negative ion mode [M-H]<sup>-</sup>). Reactions were initiated upon addition of 500 µM H<sub>2</sub>O<sub>2</sub> to a solution containing 10 µM enzyme and  $500 \, \mu M$  substrate, incubated at 25 °C for 5 min, and then quenched with excess KCN. The representative total ion chromatogram for each substrate can be found in Figs. S3 and S4, and products were characterized by the respective m/z of the (M-H)<sup>-</sup> ion with the results summarized in Tables S1 and S2. The oxidation of each substrate led to the formation of different monomeric products and oligomers with n up to 6, with varying degrees of oxidation and dehalogenation. Based on the chemical formula of each of the monomeric products, a pattern was observed in the oxidation of the substrates (with exception of 2,6-DBP) where two different pathways were present: A) insertion of one or two oxygen atoms, and B) dehalogenation and oxygen insertion (up to four oxygen atoms), with further oxidation also observed in both pathways.

# 3.3. <sup>18</sup>O-labeling studies by LC-MS

In order to characterize the origin of the O-atom incorporated in the monomeric products formed from the oxidation of 2,4- and 2,6-dihalophenols, two representative substrates were chosen for  $^{18}O$  labeling studies: 2,4-DCP and 2,4-DBP. The labeled oxygen reactions were performed with either labeled  $H_2^{18}O$  and/or labeled  $H_2^{18}O_2$  (98% and 90% enriched, respectively), and analyzed by LC-MS (negative ion mode [M-H] $^-$ ). Isotopic distributions were normalized with respect to the most intense peak, and retention times, peak distributions and m/z shifts were evaluated under each of the following four labeling conditions: 1) unlabeled  $H_2O_2$  and  $H_2O_2$  and  $H_2O_2$  and  $H_2O_3$  and  $H_3O_3$  and

The results and corresponding reaction schemes for 2,4-DCP and 2,4-DBP oxidation as catalyzed by ferric DHP B are as follows:

### 3.4. 2,4-Dibromophenol

The reaction for the ferric DHP B catalyzed oxidation of 2,4-DBP (1) was analyzed via HPLC (Fig. 1) and LC-MS (Fig. S3C), which showed the formation of multiple products (Table S1). The majority of the product peaks corresponded to oligomers (n up to 6) of various degrees of oxidation and dehalogenation. Additionally, six single-ring products were also identified. While the presence of oligomeric products suggests radical-based chemistry, this is in contrast to the results above that showed no significant effect on product distribution in the presence of radical scavengers. Possible explanations could include: i) air oxidation of products, although anaerobic studies performed on related haloguaiacol substrates still showed oligomeric products [46]; ii) the radical scavengers employed were not well-matched to scavenging the dihalophenoxyl radicals generated here; iii) the substrate radicals remain associated with DHP at the entrance of the active site, thus enabling oligomer formation without inhibition from radical scavengers; and/or iv) that the scavengers used in this study were not well suited to detecting the radicals involved.

As mentioned above, two pathways were observed in the formation of these products, which were corroborated by  $^{18}$ O labeling studies (Scheme 1). The total ion chromatograms with the peak ratios (normalized to the most intense peak) and corresponding m/z values, as well as proposed formulas, for each product can be found in Figs. S5 and S6. Predicted peak shifts and ratios, using the binomial approach, for each of the monomeric products proposed in Scheme 1 can be found in Fig. S9 [71].

# 3.4.1. Pathway A

The oxidation of the substrate proceeds through the insertion of an oxygen atom, most likely in the ortho- position since no dehalogenation was observed: i) the product 1a has a monoisotopic peak at m/z of 265 and a typical 1:2:1 isotopic distribution associated with the presence of two bromine atoms (Fig. 2A); ii) the H<sub>2</sub><sup>18</sup>O labeled reaction (Fig. 2B) showed a peak shift (+2-4 Da) and ratio consistent with the addition of one to two <sup>18</sup>O atoms predicted by theoretical calculations (note: the unlabeled <sup>79</sup>Br<sub>2</sub> isotopomer is at or below the background noise level); iii) in the  $H_2^{18}O_2$  labeled reaction (Fig. 2C) no change in the m/z or peak ratio was observed compared to the unlabeled reaction; and iv) the results for the  $H_2^{18}O/H_2^{18}O_2$  doubly-labeled reaction (Fig. 2D) were virtually identical to the predicted peak shifts and ratios (Fig. S9, 1A), and also showed the same peak shift and ratio as compared to the  $H_2^{18}O$ singly-labeled reaction. These results are consistent with a peroxidase mechanism, where substrate oxidation leads to the incorporation of an oxygen from solvent water.

Another species was found in pathway A, where a second oxygen insertion was observed, forming product 1b (Fig. S5). This product has a monoisotopic m/z of 281, and the isotopic distribution consistent with the presence of two bromine atoms. Even though the  $H_2^{18}O$  labeled reaction (Fig. S5B) showed peak shifts of +2–6 Da (incorporation of one to three  $^{18}O$  atoms), the  $^{18}O$  labeling studies suggested that the second oxygen incorporated originates from  $H_2O_2$ . Specifically, i) in the  $H_2^{18}O_2$  labeled reaction (Fig. S5C), there are peak shifts of +2–6 Da, consistent with insertion of one to three  $^{18}O$  atoms, and ii) the peak distribution observed in the  $H_2^{18}O_2$  singly-labeled reaction is closest to the peak distribution observed in the  $H_2^{18}O/H_2^{18}O_2$  doubly-labeled reaction (Fig. S5D), which also agrees with the predicted theoretical calculations (Fig. S9, 1B). These findings suggest that a peroxygenase mechanism is taking place on the second oxygen incorporation, where the oxygen is derived from  $H_2O_2$ .

A third product observed in Pathway A is 1c (Fig. 2, panels *E*-H), which has a monoisotopic peak at m/z of 279, with a peak distribution consistent with the presence of two bromine atoms. The observed

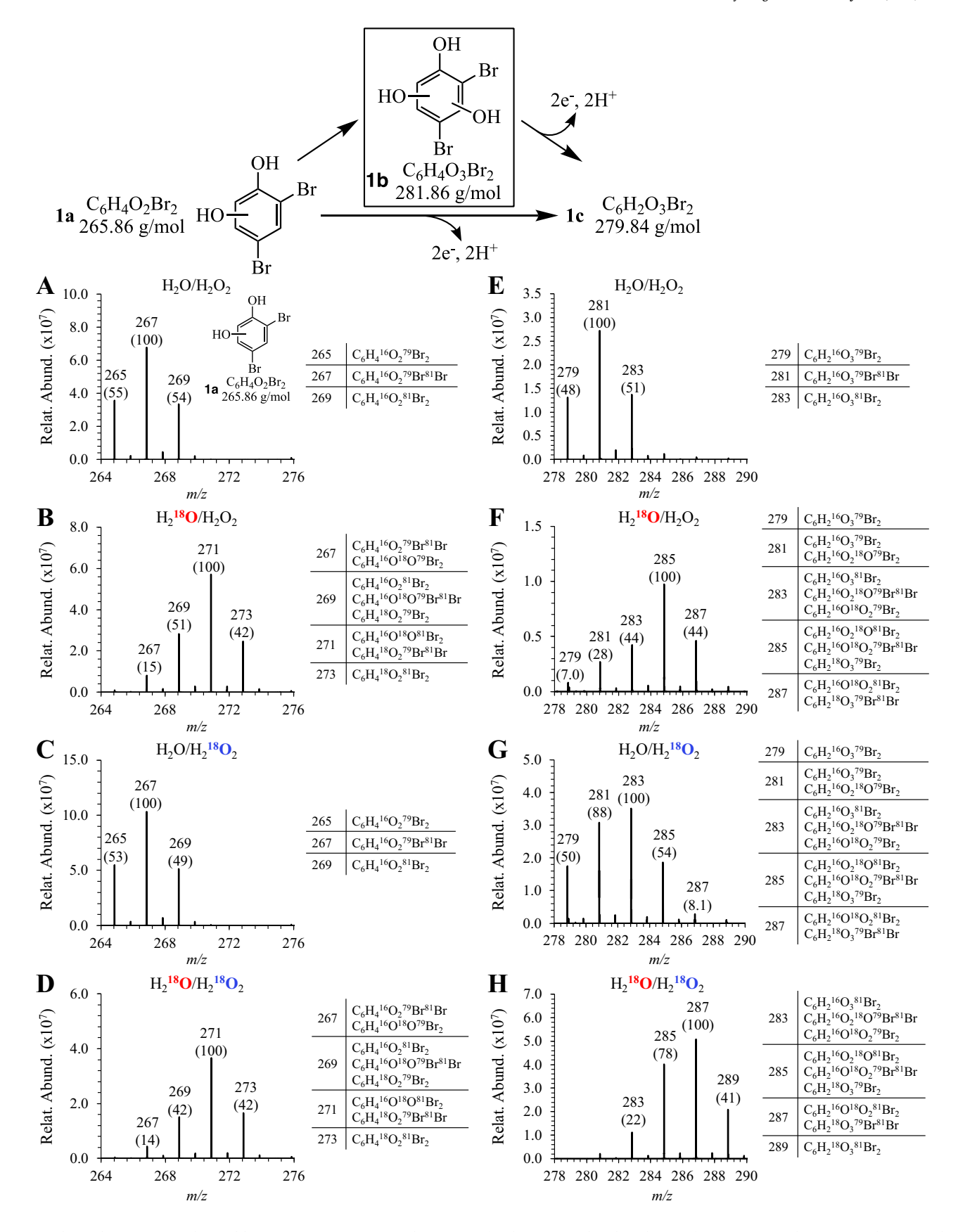


Fig. 2. Total ion chromatogram obtained by LC-MS (negative ion mode [M–H] $^-$ ) for the DHP-catalyzed oxidation of 2,4-DBP to product 1a (panels A-D) and its subsequent oxidation to product 1c (panels *E*-H). Observed peaks are labeled with the corresponding m/z and peak ratios are in parenthesis. Product 1b (box) is observed as an intermediate and data can be found on Fig. S5. A) H<sub>2</sub>O/H<sub>2</sub>O<sub>2</sub>, B) H<sub>2</sub><sup>18</sup>O/H<sub>2</sub>O<sub>2</sub>, C) H<sub>2</sub>O/H<sub>2</sub><sup>18</sup>O<sub>2</sub>, and D) H<sub>2</sub><sup>18</sup>O/H<sub>2</sub><sup>18</sup>O<sub>2</sub>. Reaction conditions: 10 μM ferric DHP B, 500 μM substrate, 500 μM H<sub>2</sub>O<sub>2</sub>, 5% MeOH/ 5 mM KP<sub>1</sub> (v/v), pH 7, 25 °C, 5 min.

Scheme 1. Proposed pathways for the H<sub>2</sub>O<sub>2</sub>-dependent DHP-catalyzed oxidation of 2,4-dibromophenol.

isotopic distribution of the three products confirms that there are no oxidative dehalogenation reactions occurring in pathway A. The oxidation of product 1a to 1c is likely taking place by a combination of peroxidase and peroxygenase mechanisms, although we cannot rule out a non-enzymatic pathway for the formation of 1c after product 1b is formed. The results for the  $\rm H_2^{18}O/H_2^{18}O_2$  labeled reaction (Fig. 2H) showed the correct peak ratio and distribution as predicted by theoretical calculations (Fig. S9, 1C). Even though both the singly labeled  $\rm H_2^{18}O_2$  or  $\rm H_2^{18}O$  reactions (Fig. 2F and G, respectively) also showed peak shifts (+2–6 Da) corresponding to the incorporation of one to three  $\rm ^{18}O$  atoms, the labeling was incomplete when compared to the  $\rm H_2^{18}O/H_2^{18}O_2$  doubly-labeled reaction.

As to the origin of the +6 Da species for 1b (Fig. S5C and S5D) and 1c (Fig. 2F and G), we surmise that scrambling of the phenolic- $^{16}$ OH occurs upon peroxidase-based oxidation of 1 in labeled  $\mathrm{H}_2^{18}$ O. This is supported through comparison of the isotopomer intensities that show additional label incorporation (without an accompanying increase in the number of O-atoms incorporated) when comparing  $\mathrm{H}_2^{18}$ O-only and the  $\mathrm{H}_2^{18}$ O/ $\mathrm{H}_2^{18}$ O<sub>2</sub> doubly-labeled reactions (i.e., Fig. 2B and D for 1a, Fig. S5B and S5D for 1b, and Fig. 2F and H for 1c). No such scrambling of the O-atom incorporated through peroxygenase activity was observed.

# 3.4.2. Pathway B

The oxidation of 2,4-DBP to product 1d indicated that oxidative dehalogenation occurred. As the phenoxyl radical could have promoted dehalogenation in either the ortho- or para- positions of the ring, the exact chemical structure of this product was ambiguous. Nevertheless, the <sup>18</sup>O-labeling results suggested that the oxygen inserted originated from a H<sub>2</sub>O molecule: i) the unlabeled reaction (Fig. S6A) shows that product 1d has a monoisotopic peak at m/z of 187 and an isotopic distribution of 1:1, characteristic of the presence of a single bromine atom; ii) the peak shifts observed in the H<sub>2</sub><sup>18</sup>O labeled reaction (Fig. S6B) of +2-4 Da are consistent with insertion of 1-2 oxygen atoms; iii) the peak ratios and distribution observed in the  $H_2^{18}O_2$  labeled reaction (Fig. S6C) are unchanged from the unlabeled reaction; and iv) the observed peak distribution and ratio are virtually identical in the H<sub>2</sub><sup>18</sup>O/H<sub>2</sub><sup>18</sup>O<sub>2</sub> doublelabeled reaction (Fig. S6D) when compared to the H<sub>2</sub><sup>18</sup>O singly-labeled reaction and the calculated data (Fig. S9, 1D). This suggests that a peroxidase mechanism is taking place in the formation of the monohalogenated diol product 1d.

### 3.5. 2,4-Dichlorophenol

### 3.5.1. Pathway A

The oxidation of 2,4-DCP initially proceeds through insertion of an oxygen atom, most likely in the ortho-position: i) in the unlabeled reaction, the total ion chromatogram of product 2a shows the typical 9:6:1 isotopic distribution expected for the presence of two chlorine atoms, with m/z for the monoisotopic peak at 177 (Fig. S7A, left); ii) the  $H_2^{18}O$ labeled reaction (Fig. S7B, left) showed a peak shift (+2-4 Da) and ratio consistent with the addition of one to two <sup>18</sup>O atoms predicted by theoretical calculations; iii) the H<sub>2</sub><sup>18</sup>O<sub>2</sub> labeled reaction (Fig. S7C, left) showed virtually no change in the m/z or peak ratio compared to the unlabeled reaction; iv) the results obtained for the  $H_2^{18}O/H_2^{18}O_2$  doublylabeled reaction (Fig. S7D, left) were virtually identical to the theoretically predicted peak shifts and ratios (Fig. S10, 2A), and also showed the same peak distribution and ratio as compared to the H<sub>2</sub><sup>18</sup>O singlylabeled reaction. These results are consistent with a peroxidase mechanism where the oxygen inserted into the substrate comes from a water molecule.

Product 2a likely undergoes further oxidation to form product 2c, which has a monoisotopic peak m/z at 191 (Fig. S7A, right), and the typical isotopic distribution expected by the presence of two chlorine atoms. These findings support that no oxidative dehalogenation reactions are occurring in pathway A. Both the  $\rm H_2^{18}O_2$  labeled reactions (Fig. S7B and C, right, respectively) showed peak shifts consistent with the insertion of one to three  $^{18}O$  atoms (+2–6 Da), however, based on the predicted peak distribution by theoretical calculations (Fig. S10, 2C), the labeling was incomplete. Only in the  $\rm H_2^{18}O_2$  doubly-labeled reaction (Fig. S7D, right) was the correct peak distribution observed, which indicates that this secondary oxidation probably proceeds through a combination of peroxidase (electron transfer) and peroxygenase (oxygen insertion) mechanisms. Product 2b was not observed in pathway A, but is proposed as an intermediate in Scheme 2 based on the data obtained for 2,4-DBP (vide supra).

# 3.5.2. Pathway B

The oxidation of 2,4-DCP to product 2d involves both oxygen insertion and dehalogenation. Resonance structures of the phenoxyl radical place the radical at the *ortho*- or *para*- position, thus the dehalogenation and oxygen insertion can take place at either the *ortho*- or *para*- position, which precludes the determination of the exact chemical

OH CI DHP 
$$H_2O_2$$
,  $H_2O$  CI CI CI CI  $H_2O_2$ ,  $H_2O$  A B OH  $H_2O_2$ ,  $H_2O$  CI  $H$ 

Scheme 2. Proposed pathways for the H<sub>2</sub>O<sub>2</sub>-dependent DHP-catalyzed oxidation of 2,4-dichlorophenol.

structure of this product. The labeling results are as follows: i) for the unlabeled reaction, the chromatogram of diol product 2d (Fig. S8A, left) shows a monoisotopic peak at m/z of 143 and an isotopic distribution of 3:1, consistent with the presence of one chlorine atom: ii) the results of the  $H_2^{18}$ O labeled reaction (Fig. S8B, left) showed a peak shift (+2–4 Da) and ratio consistent with the addition of one to two <sup>18</sup>O atoms as predicted by theoretical calculations (Fig. S10, 2D); iii) the H<sub>2</sub><sup>18</sup>O<sub>2</sub> labeled reaction (Fig. S8C, left) showed virtually no change in the m/z or peak ratio compared to the unlabeled reaction; and iv) the H<sub>2</sub><sup>18</sup>O/H<sub>2</sub><sup>18</sup>O<sub>2</sub> doubly-labeled reaction (Fig. S8D, left) showed the same peak distribution and ratio as compared to the H<sub>2</sub><sup>18</sup>O singly-labeled reaction, which is consistent with a peroxidase mechanism (the oxygen inserted is derived from a solvent water). Further oxidation of 2d to product 2e (Fig. S8A, right) was also observed, whose monoisotopic m/z of 157 and isotopic ratio were consistent with the presence of one chlorine atom, and suggests an oxidative dehalogenation reaction occurring in pathway B. Similar to the formation of product 2c, the labeling of product 2e was incomplete: both the H<sub>2</sub><sup>18</sup>O and H<sub>2</sub><sup>18</sup>O<sub>2</sub> singly-labeled reactions (Fig. S8B and C, right, respectively) showed peak shifts (+2-6 Da) consistent with insertion of one to three <sup>18</sup>O atoms compared to the unlabeled reaction, but did not match the predicted peak distribution from theoretical calculations (Fig. S10, 2E). Again, only in the H<sub>2</sub><sup>18</sup>O/H<sub>2</sub><sup>18</sup>O<sub>2</sub> doubly-labeled reaction (Fig. S8D, right) was the correct peak distribution observed, indicating that a combination of peroxidase (electron transfer) and peroxygenase (oxygen insertion) mechanisms were occurring for the formation of product 2e.

As dehalogenation has been observed via a peroxidase mechanism in DHP for 2,4,6-TXP (X = Br and Cl) substrates, it is reasonable to suggest that the dehalogenation of 2,4-DCP and 2,4-DBP is also occurring during the peroxidase step [12,18,20,23,37]. The peroxidase chemistry previously observed for DHP produces a transient, radical-containing product [9,17,20,23,72]. Dehalogenation of 2,4,6-TXP has been attributed to the radical in the *para*- position, yielding the corresponding 2,4-dihaloquinone product. As mentioned above, in the case of 2,4-DXP, either the *ortho*- or *para*- radicals could direct the dehalogenation chemistry. Formation of products 1d (2,4-DBP) and 2d (2,4-DCP) in pathway B could follow the same mechanism as TCP oxidative-dehalogenation, with selective reactivity at the *para*- position. However, because the halogen atoms reside in both *ortho*- and *para*- positions, either one could potentially be reactive. Following this logic, the site of oxygen atom incorporation could also be *ortho*- or *para*-directed in 1d and 2d,

resulting in the possibility of multiple constitutional isomers, and no further attempts were made to identify the exact molecular structure of the oxidation products.

### 3.6. Substrate binding studies

Optical difference spectra were recorded per literature protocol as a function of substrate concentration (0.21–750 eq; Figs. S11 and S12), where the spectrophotometer was referenced against a solution of 10  $\mu M$  DHP in 100 mM KP $_{\rm i}$  (pH 7) and 5% MeOH [60]. Perturbation of the Soret band was analyzed by nonlinear regression plots to provide a calculated  $A_{max}$  value, which in turn was used to calculate  $\alpha$  for the average  $\Delta A$  for each substrate. A second nonlinear regression plot provided the apparent dissociation constants ( $K_{\rm d}$ ) for all substrates studied (Table 3).

As shown in Table 3, DHP had the strongest affinity for 2,4-DCP (Kd = 29  $\pm$  1  $\mu M)$  and 2,4-DBP (K  $_d$  = 6.5  $\pm$  0.6  $\mu M)$  among the dihalophenol substrates. In fact, the low  $K_d$  values obtained for 2,4-DBP and 2,4-DCP show that they bind the tightest among all substrates and ligands examined with DHP to-date. Notably, the K<sub>d</sub> values for 2,4-DBP and 2,4-DCP are lower than those for known i) peroxygenase substrates: the 5substituted halogenated indoles (e.g., 5-Br-indole: 150 µM) [40], nitrocontaining phenols (e.g., 4-NO2-phenol: 262 µM) [41], 4-X-o-cresols (e.g., 4-Br-C: 86 μM) [42]; ii) peroxidase substrates 4-nitrocatechol (40  $\mu$ M) [41], 4-X-o-guaiacols (e.g., 4-Br-o-guaiacol: 374  $\mu$ M) [46], and 2,4,6-TCP (208  $\mu$ M) [70]; iii) the inhibitor 4-BP ( $K_d = 305 \mu$ M,  $K_i = 0.15$  $\pm$  0.03 mM) [36,48]; and iv) azole ligands [47] that bind directly to the heme-Fe. The trend in K<sub>d</sub> observed for the 2,4-dihalophenol series as a function of halogen size (F > > Cl > Br) has been observed previously [40,42,46], where the larger halogens have a strong affinity for the Xe1 hydrophobic cavity inside the binding pocket (see structural studies) [49]. Interestingly, for the 2,6-dihalophenol series, the substrates have a very poor binding affinity with DHP, and the halogen atom trend is reversed, a likely consequence of steric clashes that prevent access of the substrate to the Xe1 cavity.

Another method for comparing the binding affinities of the substrates to DHP is through use of the heme-fluoride binding competition assay (Table 3) [36]. In this method, substrates that bind tightly to the interior of the DHP active site lead to a decreased binding affinity of fluoride to the heme ( $K_1^{E^-} = 4.51 \pm 0.4$  mM), which means that the tighter the substrate binds, the higher the  $K_1^{E^-}$  will be [36]. This method is useful as some substrates, such as 2,4,6-TBP, do not exhibit substrate-

**Table 3** Dissociation constants ( $K_d$ ) for substrate binding to ferric WT DHP B at pH 7.

Substrate	<i>K</i> <sub>d</sub> (μM)	K <sub>d</sub> <sup>F-</sup> (mM) [36]	References
Dihalophenols <sup>a</sup>			
2,4-difluorophenol	1870 ( $\pm$ 150)	_	[36] <sup>b</sup>
2,4-dichlorophenol	29.3 ( $\pm$ 1.3)	74.1 (± 4.3)	[36] <sup>b</sup>
2,4-dibromophenol	6.4 ( $\pm$ 0.6)	$172.1 (\pm 9.0)$	[36] <sup>b</sup>
2,6-difluorophenol	1940 (± 490)	1/2.1 (± 9.0)	[36] <sup>b</sup>
2,6-dichlorophenol		-	
· ·	2400 (± 430)	-	[36] <sup>b</sup>
2,6-dibromophenol	$\sim 7100 \ (\pm \ 3600)^{c}$	$5.7~(\pm~0.5)$	[36] <sup>b</sup>
mt t			
Phenols			
Pentachlorophenol	79 (± 9)	-	[42]
2,4,6-tribromophenol	-	$23.8~(\pm~1.0)$	[36]
2,4,6-trichlorophenol	$208~(\pm~13)$	14.5 ( $\pm$ 0.8)	[70]
4-bromophenol	$305~(\pm~15)$	$12.3~(\pm~0.8)$	[70]
4-nitrophenol	$262 (\pm 23)$	-	[41]
2,4-dinitrophenol	$105~(\pm~21)$	_	[41]
4-nitrocatechol	40 ( $\pm$ 1)	-	[41]
Haloindoles			
5-Cl-indole	$317~(\pm~23)$	$8.6~(\pm~0.3)$	[36,40]
5-Br-indole	150 (± 10)	$13.2~(\pm~0.5)$	[36,40]
5-I-indole	$62 (\pm 10)$	$16.8~(\pm~0.4)$	[36,40]
5-1-mdoic	02 (± 10)	10.0 (± 0.4)	[50,40]
Azoles			
Imidazole	52 (± 2)		[47]
Benzotriazole		_	
	82 (± 2)	-	[47]
Benzimidazole	110 ( $\pm$ 8)	-	[47]
Guaiacols			
4-F-o-guaiacol	$2430 (\pm 210)$	-	[46]
4-Cl-o-guaiacol	493 ( $\pm$ 53)	-	[46]
4-Br-o-guaiacol	$374 (\pm 42)$	-	[46]
o-guaiacol	14,700 ( $\pm$ 720)	$8.0~(\pm~0.3)$	[36,46]
Cresols			
4-F-o-cresol	2970 ( $\pm$ 390)	-	[42]
4-Cl-o-cresol	130 (± 4)	_	[42]
4-Br-o-cresol	86 (± 14)	_	[42]
p-cresol	2680 (± 380)	$7.4~(\pm~0.4)$	[36,42]

 $<sup>^</sup>a$  Conditions. [enzyme] = 10  $\mu M,\,0.21\text{--}750$  equiv. substrate, 5% MeOH, 100 mM KP $_i$  pH 7.

dependent shifts in their UV–visible spectra upon binding to DHP, likely due the binding of TBP deep in the hydrophobic cavity of DHP, which has been previously observed via X-ray crystallography. The consequence of this binding motif is that it does not perturb the 5-coordinate (5c)/6-coordinate (6c) equilibrium binding of water to the heme that is being typically probed by the optical difference spectra in Figs. S11 and S12, yet it does impact the binding of fluoride to the heme-Fe. A comparison of the  $K_{\rm d}^{\rm F}$  values at pH 7 reveals that 2,4,6-TBP binding is stronger than the inhibitor 4-BP, yet weaker than 2,4-DCP and 2,4-DBP substrates, resulting in the substrate binding affinity order: 4-BP < 2,4,6-TBP < 2,4-DBP. In addition, the low  $K_{\rm d}^{\rm F}$  (5.7 mM) observed for 2,6-DBP shows that this substrate has a very low affinity for the protein [36], which was confirmed by the present study.

With respect to the p $K_a$  values of 8.05, 7.86 and 6.89 for 2,4-DCP, 2,4-DBP and 2,6-DBP, respectively, the data suggest that binding occurs when the substrates are predominately in their neutral or partly ionized (2,6-DBP) phenolate form in pH 7.0 buffer. Structural elements of the DHP active site involving H-bonding, aromatic  $\pi$ - $\pi$  stacking and hydrophobic interactions to 2,4-DCP and 2,4-DBP that lead to such strong binding affinities were elucidated by X-ray crystallography.

### 3.7. Protein crystallization and X-ray diffraction studies

Incubation of non-His tagged DHP B crystals with the ligands [4-XP, 2,4-DXP (X = Cl, Br) and 2,6-DXP (X = F, Cl, Br)] successfully yielded the DHP B-ligand complexes as determined by X-ray crystallographic diffraction methods. The X-ray data collection and refinement statistics for the structures are provided in Tables S3 and S6. DHP B crystallized as a homo-dimer in the asymmetric unit of space group  $P2_12_12_1$ , consistent previous crystal structures of this [24,39,41,42,46,47,49,56,64,73]. The protomer environments were found to be identical within each structure, in particular the orientation of the ligand binding site within the DHP B distal cavity. All distances provided for 4-XP and 2,4-DXP (X = Cl, Br) are an average between the two protomers, and those for 2,6-DXP (X = F, Cl, Br) are from protomer B (Tables S4 and S5, respectively). The ligand binding site orientations are shown in Figs. 3 and S16.

Two binding orientations were determined for 2,4-DCP from crystals isolated from the same mother liquor, labeled with respect to their proximity to the heme  $\alpha$  and  $\beta$  edges as 2,4-DCP $_{\alpha}$  (PDB: 7LZN, Fig. 3A) and 2,4-DCP<sub>6</sub> (PDB: 7LZK, Fig. 3B). The position of 2,4-DCP<sub>\alpha</sub> shows the molecule is bound 4.1 Å above the heme, between the Fe and the  $\alpha$  edge, with its hydroxyl group directed towards the Fe (4.9 Å). The aromatic ring of F21 is oriented for  $\pi$ - $\pi$  stacking interactions with the substrate, F60 is displaced to accommodate the p-Cl atom (displacement can be observed in Fig. 3C), which is directed towards the Xe1 hydrophobic binding cavity [49], and the o-Cl is directed deep in the heme cavity. The distal histidine, H55, was found in the "closed" conformation, with its N<sup>E</sup> at a H-bonding distance of 2.5 Å from the substrate OH group, further stabilizing 2,4-DCP $_{\alpha}$  in the binding cavity (Fig. 3A). The 2,4-DCP $_{\beta}$ binding site orients the molecule above the heme, between the Fe and  $\beta$ edge. The  $O^{\gamma}$  of T56 is rotated into the distal pocket interacting with the OH group of 2,4-DCP<sub>β</sub> at a hydrogen bonding distance of 2.8 Å. The o-Cl atom is pointed down, oriented towards the entrance of the pocket 3.4 Å away from propionate group D, and the p-Cl is positioned internally (Fig. 3B). Due to the proximity to the pocket entrance, H55 is found in the solvent-exposed "open" conformation. For comparison, a superimposed structure of 2,4-DCP $_{\alpha}$  and 2,4-DCP $_{\beta}$  shows that they occupy completely different positions in the pocket (Fig. 3C). Moreno-Chicano and co-workers have recently determined the structure of DHP B complexed with 2,4-DCP (PDB: 6I7F) by serial femtosecond X-ray crystallography (SFX) [44]. The authors observed only one binding position for 2,4-DCP, which was virtually identical to the observed position for 2,4- $DCP_{\alpha}$ , shown as a superimposed structure (Fig. S15A).

The structure of DHP B complexed with 2,4-DBP (PDB: 7LZO) shows a single binding site in the distal cavity for this substrate (Fig. 3D) and the superimposed crystal structure of 2,4-DBP and 2,4-DCP $_{\alpha}$  (Fig. S15B) shows that both these substrates occupy nearly identical positions in the binding site, and, interestingly, is virtually the same position as to that observed previously for 4-Br-o-cresol (PDB: 6ONX, Fig. S15C) [42]. The structures here obtained for 2,4-DCP, 2,4-DBP, 4-CP and 4-BP for DHP B were also compared to previously published structures of 2,4,6-TCP (PDB: 4KMV and 4KMW) and 2,4,6-TBP (PDB: 4FH6) complexed with DHP A (Figs. S15D-F) [24,38].

The binding sites for the 4-halophenol series (4-XP, X = F, Cl, Br, I) have been previously elucidated by X-ray crystallography in DHP A [35]. For comparative purposes, the 4-CP (PDB: 7M0H, Fig. 3E) and 4-BP (PDB: 7M0F, Fig. 3F) complexes with DHP B were structurally characterized here by X-ray crystallography. The 4-CP structure was found to bind in a similar orientation to 2,4-DCP $_{\beta}$ , observed above the heme, positioned between the Fe and  $\beta$  edge, resulting in H55 exclusion from the distal pocket in the "open" conformation (Fig. 3E). The Cl atom is positioned internally, while the OH group is directed towards the cavity opening at a H-bonding distance of 2.7 and 3.4 Å from the heme propionate group D and Y38 residue, respectively. In contrast to the halogen-differentiated structures of 2,4-DCP $_{\alpha}$  and 2,4-DCP $_{\beta}$ , the DHP B–4-BP (Fig. 3F) shows that substituting Cl with the larger Br bears no

<sup>&</sup>lt;sup>b</sup> This work.

<sup>&</sup>lt;sup>c</sup> Estimated *K*<sub>d</sub> based on experimental data.

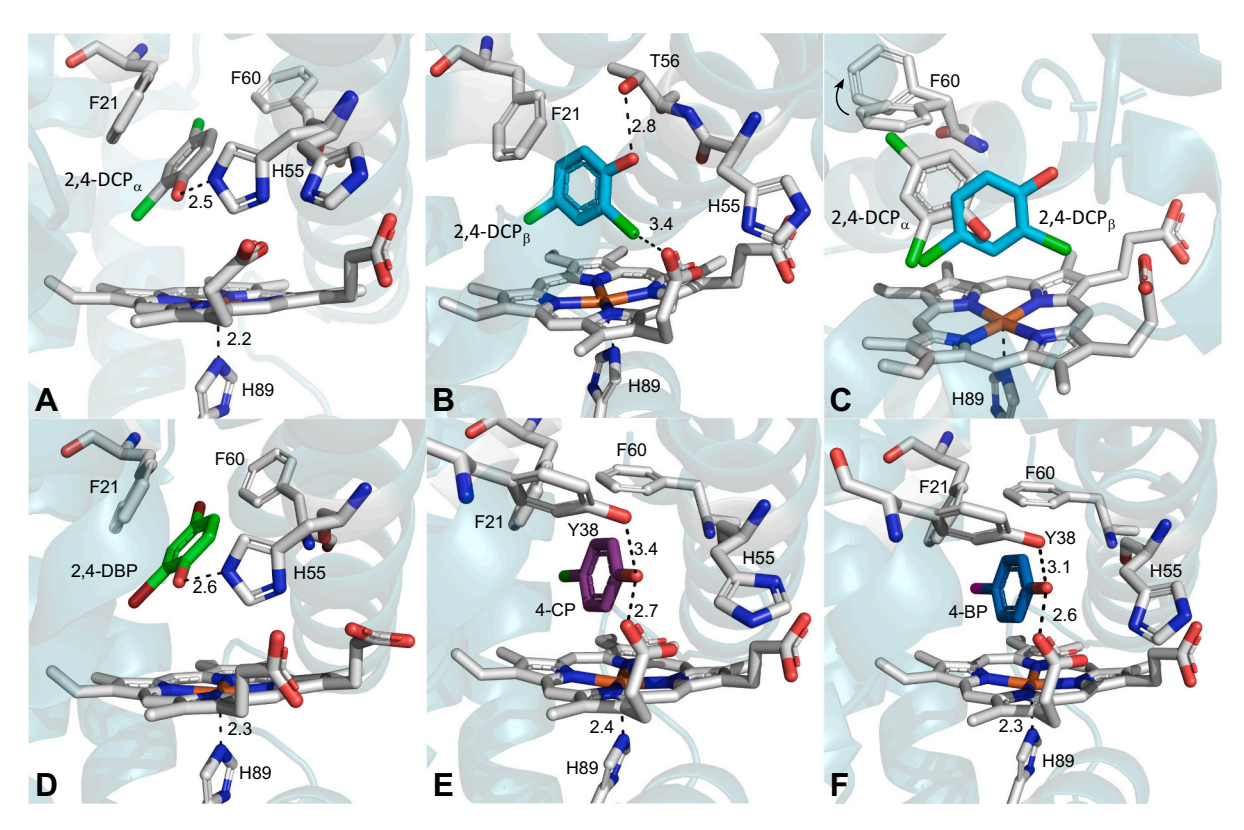


Fig. 3. X-ray crystal structures depicting the halophenol binding sites within the distal pocket of DHP B. A) 2,4-DCP $_{\alpha}$  (grey, PDB: 7LZN), B) 2,4-DCP $_{\beta}$  (cyan, PDB: 7LZK), C) Superposition of 2,4-DCP $_{\alpha}$  and 2,4-DCP $_{\beta}$  binding sites, D) 2,4-DBP (green, PDB: 7LZO), E) 4-CP (purple, PDB: 7MOH) and F) 4-BP (blue, PDB: 7MOF). (For interpretation of the references to colour in this figure legend, the reader is referred to the web version of this article.)

consequence on binding orientation, reflected in the observation of 4-BP residing in virtually the same orientation as 4-CP (PDB: 7M0F, Fig. 3F). The only noticeable difference in the distal environment is that 4-BP is located slightly higher above the heme, reflected in a shorter H-bonding distance between substrate hydroxyl group and Y38 (3.1 Å). Moreover, analysis of 4-CP and 4-BP binding sites with respect to DHP A [35] and DHP B yielded virtually identical orientations (data not shown).

The crystal structures of DHP B complexed with the 2,6-DXP series (X = F, Cl, Br) were also elucidated (Fig. S16), and all three substrates were found to bind inside the distal cavity. The distances provided are for protomer B (Table S5), and X-ray data collection and refinement statistics are provided in Table S6. The structure obtained for 2,6-DFP (PDB: 7M1K, Fig. S16A) shows that the substrate is positioned internally, away from the heme propionates [74]. The hydroxyl group of the substrate is directed towards the heme iron (4.5 Å) and forming a Hbond with  $N^{\epsilon}$  of H55 in the "closed" conformation (3.2 Å). One of the fluorine atoms is pointed internally, and the other forms two H-bonds, one with N<sup>8</sup> of H55 at a distance of 2.5 Å, and a second one with the hydroxyl of T56 at a distance of 3.1 Å [74,75]. Furthermore, F60 is displaced to its alternative position (not shown), and F21 is oriented for  $\pi$ - $\pi$  stacking interactions with the aromatic ring of the substrate. Interestingly, a nonspecific binding location was also identified for 2,6-DFP in protomer A in the proximal side of the heme cavity, with an approximate occupancy of 40% (PDB: 7M1K, Fig. S16B; see SI for more details).

For 2,6-DCP, (PDB: 7M1I, Fig. S16C) the substrate is positioned 4.1 Å above the heme center (distance between C4 and heme iron). The hydroxyl group is interacting with T56 and Y38 via hydrogen bonding (3.3 and 2.9 Å, respectively). The bulky halogen atoms may play a role in accommodating the binding position of the substrate [74,75], with one of the chlorine substituents positioned internally and interacting with T56 (2.9 Å), and the other facing the entrance of the pocket, interacting with N $^{\delta}$  of H55 in the "open" conformation and propionate D (2.6 and

2.9 Å, respectively). Additionally, 2,6-DCP was found to occupy a similar position compared to 2,4,6-TCP<sub>ext</sub>, although 2,6-DCP is rotated internally (~35°) compared to 2,4,6-TCP<sub>ext</sub>, resulting in a displacement of the two substrate OH groups by 2.2 Å (Fig. S16D). Lastly, 2,6-DBP was found present only in protomer B (PDB: 7M1J, Fig. S16E), with 70% occupancy, and a bis-histidine ligation was observed for protomer A (H55 N°-Fe-N° H89, 2.2 and 2.1 Å, respectively) (PDB: 7M1J, Fig. S16F). The substrate was found close to the heme  $\gamma$  edge near the heme propionates (the same as 2,6-DCP), but its hydroxyl group, unlike 2,6-DCP, was engaged in indirect H-bonding interactions with T56 and Y38 via a water molecule (OH-H $_2$ O 2.0 Å, H $_2$ O-Y38 2.8 Å, and H $_2$ O-T56 2.9 Å) (Fig. S17E), in agreement with its weaker binding compared to 2,6-DCP. H55 is observed in both "open" and "closed" conformations in this structure due to the partial substrate occupancy of 0.7 resulting in the accompanying alternative conformations of H55.

### 3.8. Stopped-flow studies

Single and double-mixing stopped-flow methods were used to investigate the reaction of representative substrates 2,4-DBP and 2,6-DBP with  $\rm H_2O_2$ -activated DHP (Figs. 4 and 5). Studies were conducted with pre-formed Compound I [10,11], Compound ES [13,20], Compound II [12], or with the oxyferrous species itself as the starting state. While different substrate concentrations were investigated (1, 2.5, 5 and 10 equiv), the studies presented here focus on 5 equiv. 2,4-DBP and 10 equiv. 2,6-DBP for clarity purposes. As the data did not fit kinetic models as one-step/two-species or two-step/three-species irreversible mechanisms, the experimentally obtained spectra at selected time points detailed in the figure legends are shown.

# 3.8.1. Compound I reactivity

Compound I [(Por·+)Fe<sup>IV</sup>=O; 406 (Soret), 528, 645 nm] was preformed upon reaction of ferric DHP B (Y28F/Y38F) with  $H_2O_2$  (10

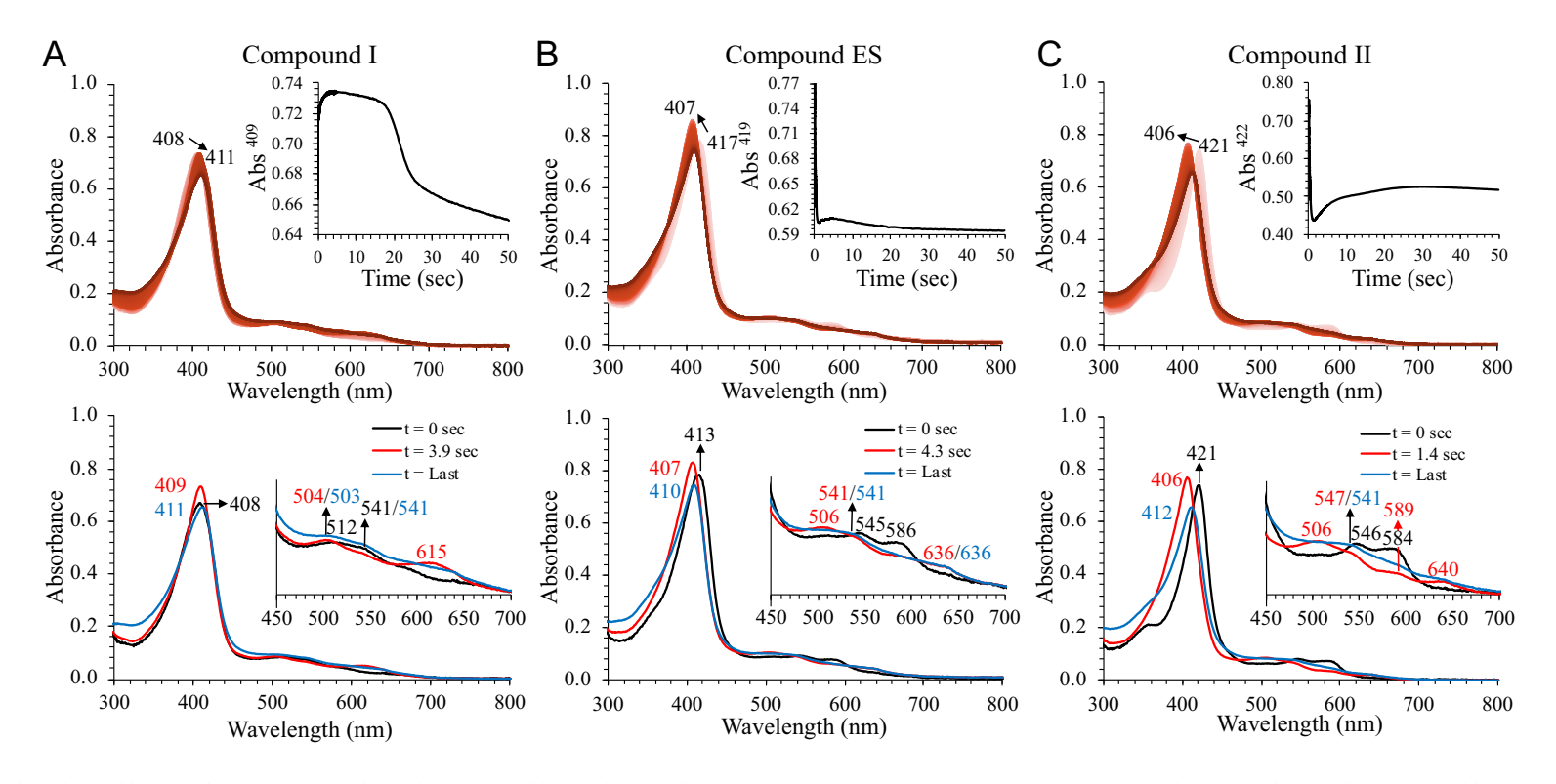


Fig. 4. Kinetic data obtained by optical spectroscopy for the oxidation of 2,4-dibromophenol in the presence of  $H_2O_2$ -activated DHP B at pH 7. A) Compound I: *Top panel*, stopped-flow UV-visible spectra of the double-mixing reaction of preformed Compound I (10  $\mu$ M), itself formed in an initial mixing step from the reaction of ferric DHP B (Y28F/Y38F) with a 10-fold excess of  $H_2O_2$  in an aging line for 75 ms, with a 5-fold excess of 2,4-dibromophenol (900 scans over 49 s); *inset*: the single-wavelength (409 nm) dependence on time obtained from the raw data. *Bottom panel*, experimentally obtained spectra of the double-mixing reaction of preformed Compound ES: *Top panel*, stopped-flow UV-visible spectra of the double-mixing reaction of preformed Compound ES (10  $\mu$ M), itself formed in an initial mixing step from the reaction of ferric WT DHP B with a 10-fold excess of  $H_2O_2$  in an aging line for 420 ms, with a 5-fold excess of 2,4-dibromophenol (900 scans over 49 s); *inset*: the single-wavelength (419 nm) dependence on time obtained from the raw data. *Bottom panel*, experimentally obtained spectra for Compound ES reacted with 2,4-dibromophenol (black, t = 0 s), its reduction to the ferric enzyme (red, t = 4.3 s) and the final spectrum (blue, t = 49 s). C) Compound II: *Top panel*, stopped-flow UV-visible spectra of the double-mixing reaction of preformed Compound II (10  $\mu$ M), itself formed in an initial mixing step from the reaction of oxyferrous WT DHP B preincubated with 1 equiv. of 2,4,6-TCP, with a 10-fold excess of H<sub>2</sub>O<sub>2</sub> in an aging line for 3.2 s, with a 5-fold excess of 2,4-dibromophenol (900 scans over 49 s); *inset*: the single-wavelength (422 nm) dependence on time obtained from the raw data. *Bottom panel*, experimentally obtained spectra for Compound II reacted with 2,4-dibromophenol (900 scans over 49 s); *inset*: the single-wavelength (422 nm) dependence on time obtained from the raw data. *Bottom panel*, experimentally obtained spectra for Compound II reacted with 2,4-dibrom

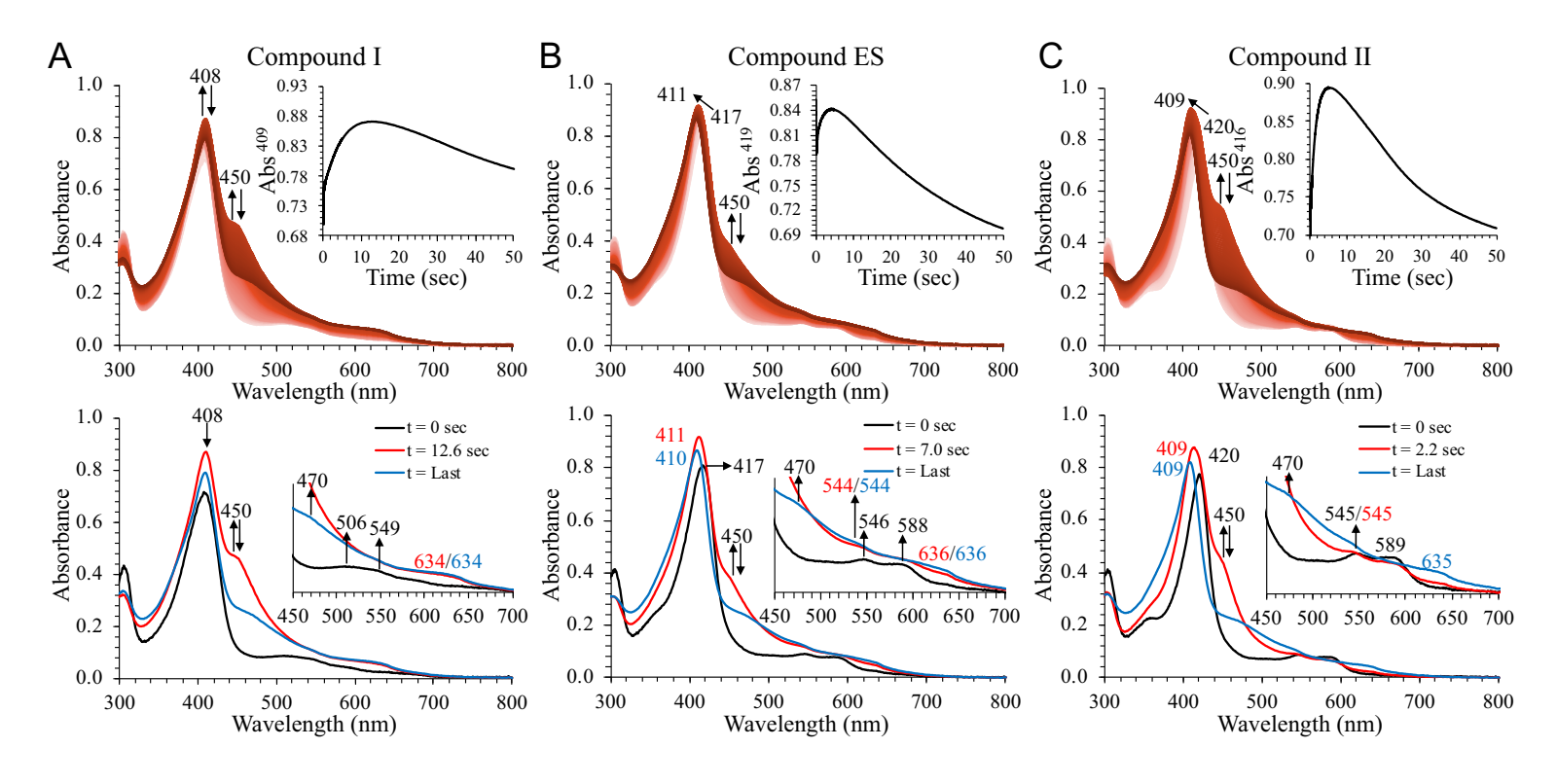


Fig. 5. Kinetic data obtained by optical spectroscopy for the oxidation of 2,6-dibromophenol in the presence of  $H_2O_2$ -activated DHP B at pH 7. Double mixing methods for reactions employing preformed Compounds I, ES, and II were as described in Fig. 4. A) Compound I: *Top panel*, stopped-flow UV-visible spectra of the reaction of Compound I (10  $\mu$ M) with a 10-fold excess of 2,6-dibromophenol (900 scans over 49 s); *inset*: the single-wavelength (409 nm) dependence on time obtained from the raw data. *Bottom panel*, experimentally obtained spectra for Compound I reacted with 2,6-dibromophenol (black, t = 0 s), intermediate species showing the 450 nm band (red, t = 12.6 s) and the final spectrum with the 470 nm feature (blue, t = 49 s). B) Compound ES: *Top panel*, stopped-flow UV-visible spectra of the reaction of Compound ES (10  $\mu$ M) with a 10-fold excess of 2,6-dibromophenol (900 scans over 49 s); *inset*: the single-wavelength (419 nm) dependence on time obtained from the raw data. *Bottom panel*, experimentally obtained spectra for Compound II: *Top panel*, stopped-flow UV-visible spectra of the reaction of Compound II (10  $\mu$ M) with a 10-fold excess of 2,6-dibromophenol (900 scans over 49 s); *inset*: the single-wavelength (416 nm) dependence on time obtained from the raw data. *Bottom panel*, experimentally obtained spectra for Compound II reacted with 2,4-dibromophenol (black, t = 0 s), intermediate species showing the 450 nm band (red, t = 2.2 s) and the final spectrum with the 470 nm feature (blue, t = 49 s). (For interpretation of the references to colour in this figure legend, the reader is referred to the web version of this article.)

equiv) in an aging line for 75 ms prior to rapid mixing (1.5 ms) with substrate, either 2,4-DBP (5 equiv) or 2,6-DBP (10 equiv), in  $100 \text{ mM KP}_i$  (pH 7) containing 5% MeOH.

- i) 2,4-dibromophenol (Fig. 4A): The first observed spectrum for 2,4-DBP did not match the spectral features for Compound I, however the observed spectrum closely matched that of ferric DHP B (Y28F/ Y38F) [408 (Soret), 512 and 541 (sh) nm]. This result suggests that Compound I rapidly reacts with the substrate within the mixing time of the stopped-flow apparatus. Within 3.9 s, a second species [409 (Soret), 504, 615 nm] was formed, which showed a slight hyperchromic shift in the Soret band in addition to a broad feature at 615 nm. As these ferric-like spectral features do not match any previously observed DHP B species, this may be possibly indicative of substrateand/or product-bound DHP B (Y28F/Y38F), however the identity of this post-reaction species was not further explored. The last spectrum [411 (Soret), 503, 540 nm] showed a slight broadening of the Soret band and a flattening of the visible bands. At longer observation times (500 s), the ferric-like enzyme converted to a species whose spectral features matched those of Compound RH [20], an inactivated form of DHP B (data not shown).
- ii) 2,6-dibromophenol (Fig. 5A): Similar to what was observed for 2,4-DBP, the first observed spectrum upon reaction of Compound I with 2,6-DBP did not match the spectral profile of Compound I. However, the observed spectrum closely matched that of ferric DHP B (Y28F/Y38F) [408 (Soret), 506 and 549 (sh) nm], again suggesting that Compound I rapidly reacts with the substrate within the mixing time (1.5 ms) of the stopped-flow apparatus. Within 12.6 s, a hyper-chromic shift in the Soret was observed along with a strong absorbance at 450 nm. While the origin of this feature was not investigated further, we surmise that it is likely an oligomeric product [e.g., poly (2,6-dibromophenol oxide)]. The last spectrum [408 (Soret), 470, 634 nm] showed the disappearance of the 450 nm band, with the appearance of a 470 nm feature. At longer observation times (500 s), Compound RH was formed (data not shown).

Thus, when Compound I [11] was reacted with either 2,4-DBP or 2,6-DBP, the first species observed was the ferric enzyme, showing complete reduction of the ferryl within the mixing time of the stopped-flow apparatus (1.5 ms), a result that has been consistently seen for all known DHP substrates (5-bromoindole [40], 4-nitrophenol [41], pyrrole [45], 4-bromo-o-guaiacol [46], and 4-bromo-o-cresol [42]).

# 3.8.2. Compound ES reactivity

Ferric WT DHP B was reacted with 10 equiv. of  $H_2O_2$  in an aging line for 420 ms to form Compound ES [(Por)Fe<sup>IV</sup>=O·Tyr38; 418 (Soret), 545, 586 nm] prior to rapid mixing (1.5 ms) with the substrate, 2,4-DBP (5 equiv) or 2,6-DBP (10 equiv), in 100 mM KP<sub>i</sub> (pH 7) containing 5% MeOH.

- i) 2,4-dibromophenol (Fig. 4B): The first observed spectrum for 2,4-DBP was a mixture between pre-formed Compound ES and ferric DHP B [413 (Soret), 506 (sh), 545, 586 nm] that reduced fully to the ferric enzyme within 4.3 s [407 (Soret), 506, 636 nm]. The final spectrum exhibited a slight broadening of the Soret and a band at 541 nm [410 (Soret), 541, 636 nm]. At longer observation times (500 s), the ferric enzyme converted to Compound RH (data not shown).
- ii) 2,6-dibromophenol (Fig. 5B): Compound ES [417 (Soret), 546, 588 nm] was the first observable species after rapid mixing with 2,6-DBP, which converted within 7.0 s to a species [411 (Soret), 450, 544 (sh), 636 nm] that exhibited the same strong 450 nm band as noted above for 2,6-DBP/Compound I. Similar to that reaction, the 450 nm band disappeared, with the appearance of a 470 nm feature. Compound RH formed at longer observation times (500 s; data not shown).

iii) The reactivity of the remaining 2,4- and 2,6-DXP (X = F, Cl) substrates was also studied under the same conditions as described above (i.e., 5 equiv. for the 2,4-dihalophenols and 10 equiv. for the 2,6-dihalophenols). The time required for each substrate to react with pre-formed Compound ES and reform the ferric species can be found in Table 4, and representative reactions can be found in Figs. S13 and S14. All substrates reduced Compound ES to the ferric enzyme, although the times varied ~7fold (4.3-29.5 s). Interestingly, the intense band at 450 nm was not observed for 2,6-DFP and 2,6-DCP, although in the case of 2,6-DCP, the broadening of the Soret band suggests the formation of a similar product that absorbs around 400 nm (Fig. S14B). A trend was observed for both 2,4- and 2,6-dihalophenol series, where the substrates with the larger halogen atoms were found to react faster with Compound ES (Br > Cl > F). Overall, the 2,6dihalophenols were slower to reduce Compound ES when compared with their respective 2,4-dihalophenols analogs (Table 4).

The Compound ES [13,14] reactivity observed here with the DXP substrates is consistent with previous studies showing that nitrophenol [41], pyrroles [45], and cresols [42], all reduced the enzyme back to the ferric state. It is important to note that these studies do not differentiate between Compound ES-mediated substrate oxidation within the active site versus at the surface of the enzyme given that the tyrosyl radical migration pathway ( $\bullet$ Tyr38  $\rightarrow \bullet$ Tyr28) in DHP B leads to a more solvent-exposed Tyr28 radical [11].

### 3.8.3. Compound II reactivity

Compound II [420 (Soret), 546, 584 nm] was preformed upon mixing 10 equiv.  $H_2O_2$  in an aging line for 3.2 s with oxyferrous DHP B that was pre-incubated with 1 equiv. of 2,4,6-TCP [12], and was then reacted (1.5 ms mixing time) with either 2,4-DBP (5 equiv) or 2,6-DBP (10 equiv) in 100 mM KP<sub>i</sub> (pH 7) containing 5% MeOH.

- i) 2,4-dibromophenol (Fig. 4C): The first species observed was Compound II [421 (Soret), 546, 584 nm], which reduced within 1.4 s to ferric DHP B [406 (Soret), 506, 541 (sh), 589 (sh), 640 nm]. The final spectrum [412 Soret, 541, 640 nm] showed a slight broadening of the Soret band with a feature at 541 nm. At longer observation times (500 s), a decrease in absorbance and broadening of the Soret band, consistent with heme bleaching, were observed (data not shown).
- ii) 2,6-dibromophenol (Fig. 5C): The first observable species was Compound II [420 (Soret), 545, 584 nm], which reduced within 2.2 s to ferric DHP B [409 (Soret), 450, 544 (sh), 635 nm] with concomitant formation of a strong 450 nm band. The final spectrum [409 (Soret), 470, 544 (sh), 635 nm] showed disappearance of the 450 nm band with the formation of the 470 nm feature. At longer observation

**Table 4**Summary of the stopped-flow UV–visible spectroscopic data for the reaction of compound ES with 2,4-and 2,6-dihalophenols at pH 7.

Substrate	Compound ES $\rightarrow$ ferric time (s)	Observed ferric species $\lambda_{max}$ (nm)
2,4- difluorophenol	13.0	409, 505, 636
2,4- dichlorophenol	6.8	409, 506, 634
2,4- dibromophenol	4.3	407, 506, 636
2,6- difluorophenol	29.5	409, 543, 638
2,6- dichlorophenol	13.0	410, 544, 636
2,6- dibromophenol	7.0	409, 545, 635

times (500 s), a decrease in absorbance and broadening of the Soret were observed, consistent with heme bleaching (data not shown).

Overall, for the oxidation of DXP by Compound II [12], conversion to the ferric enzyme was observed for both 2,4-DBP and 2,6-DBP substrates, consistent with the Compound II reactivity reported for 2,4,6-TCP [12,28], 5-Br-indole [40], pyrrole [45], 4-NO<sub>2</sub>-phenol [41], 4-Bro-guaiacol [46], and 4-Br-o-cresol [42].

# 3.8.4. Oxyferrous reactivity

In a single-mixing method, oxyferrous DHP B that was preincubated with substrate (5 and 10 equiv. for 2,4-DBP and 2,6-DBP, respectively) was rapidly reacted (1.5 ms) with 10 equiv. of H<sub>2</sub>O<sub>2</sub> in 100 mM KP<sub>i</sub> (pH 7) containing 5% MeOH (Fig. 6).

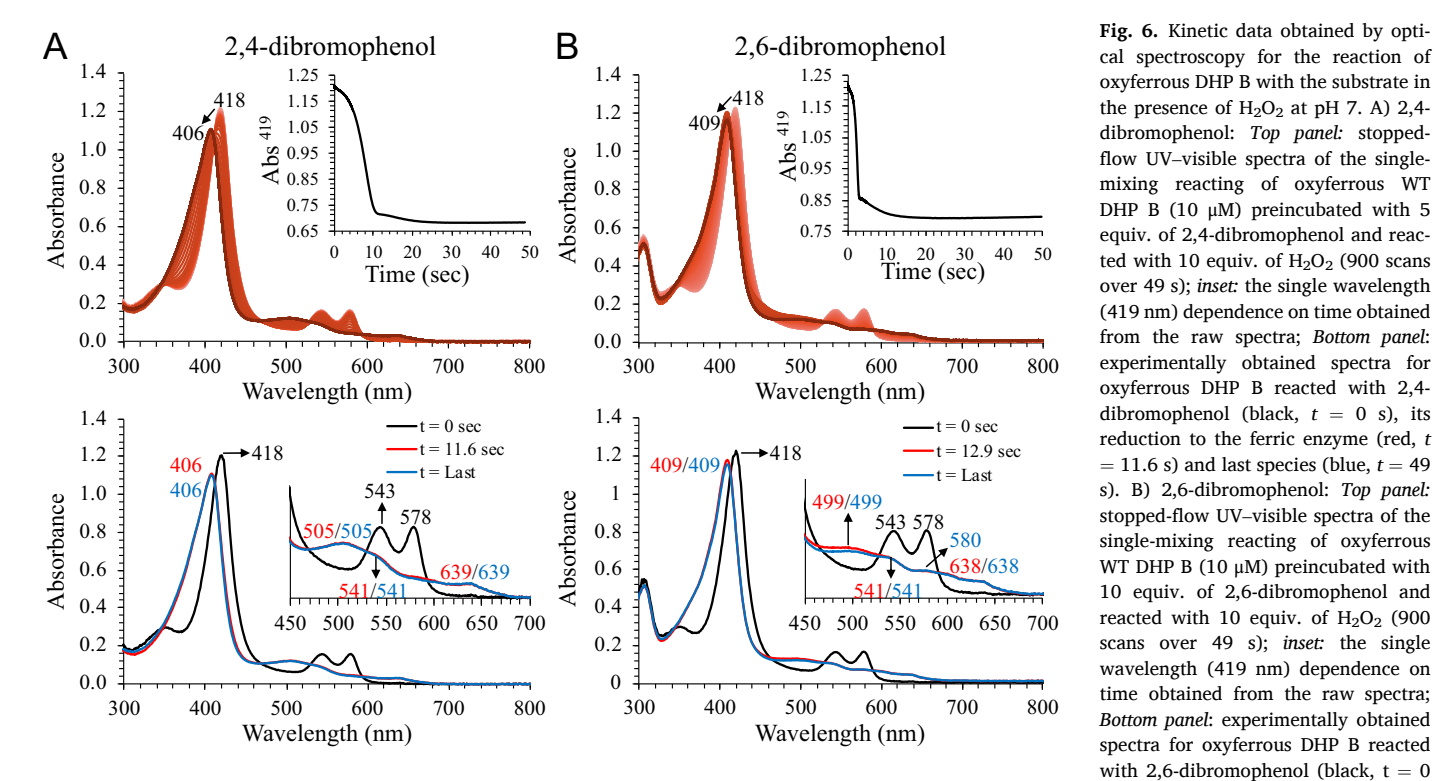
- i) 2,4-dibromophenol (Fig. 6A): The first species observed was the oxyferrous enzyme [418 (Soret), 543, 578 nm] that converted within 11.6 s to a stable ferric species [406 (Soret), 505, 541, 639]. At longer times (500 s), the last species observed was a ferric/oxyferrous mixture [405 (Soret), 509, 541, 576 nm] (data not shown).
- ii) 2,6-dibromophenol (Fig. 6B): The first observable species was the oxyferrous enzyme [418 (Soret), 543, 578 nm] that converted within 12.9 s to a stable ferric species [406 (Soret), 499, 638]. At longer times (500 s), a ferric/oxyferrous mixture [409 (Soret), 500, 540, 575 nm] was observed (data not shown).

The reactivity of oxyferrous DHP yielding the ferric enzyme did not proceed through Compound II as an observable intermediate, a similar finding to what has been reported for 4-Br-o-guaiacol [46] and 4-Br-ocresol [42] substrates, yet differs from halophenols [12], indoles [40], nitrophenol [41], and pyrroles [45]. We note the presence of isobestic points in the top panels of Fig. 6A and B as further evidence to support that the reduction is occurring in a single step.

In summary, the main observations from the stopped-flow studies with 2,4-DBP and 2,6-DBP were i) Compound I was rapidly reduced by both substrates within the 1.5 ms mixing time of the instrument to a ferric-like enzyme state; ii) Compound ES was reduced to the ferric enzyme within 4.3 and 7.0 s for 2,4- and 2,6-DBP, respectively; iii) Compound II was reduced more quickly to the ferric enzyme (within 1.4 and 2.2 s for 2,4- and 2,6-DBP, respectively) than Compound ES; iv) in the case of 2,6-DBP, a product with an intense band at 450 nm was observed in the presence of all reactive species (Compounds I, ES and II), however this product was found to be unstable, possibly forming a new product with a 470 nm absorption; and v) oxyferrous DHP reacted with both substrates in the presence of H<sub>2</sub>O<sub>2</sub> to yield ferric DHP, and at longer observation times (500 s), DHP slowly reduced back to the oxyferrous state, suggesting a product-driven reduction of the enzyme, a result that has been previously observed for DHP upon reaction with halophenols [20], indoles [40], pyrroles [45], and guaiacols [46].

### 4. Discussion

The enzymatic assays performed in the presence of DHP, substrate and H<sub>2</sub>O<sub>2</sub> demonstrate that DHP is able to catalyze the H<sub>2</sub>O<sub>2</sub>-dependent oxidation of 2,4- and 2,6-dihalophenols (DXP; X = F, Cl, Br). In the 2,4-DXP series, the percent conversion followed the order DFP > DCP > DBP, the same trend was been observed for 4-X-o-cresols (X = F, Cl, Br) [42], and opposite trend was observed for 5-X-haloindoles (X = F, Cl, Br) [40]. On the other hand, a near 100% conversion for all three 2,6-DXP substrates was observed despite employing unoptimized conditions, a finding that was also previously noted for the oxidation of 4-X-oguaiacols [46]. Multiple product peaks in the representative chromatograms for each substrate were identified as monomers with varying degrees of oxidation and dehalogenation, as well as oligomers with n up



oxyferrous DHP B with the substrate in the presence of H<sub>2</sub>O<sub>2</sub> at pH 7. A) 2,4dibromophenol: Top panel: stoppedflow UV-visible spectra of the singlemixing reacting of oxyferrous WT DHP B (10 µM) preincubated with 5 equiv. of 2,4-dibromophenol and reacted with 10 equiv. of H2O2 (900 scans over 49 s); inset: the single wavelength (419 nm) dependence on time obtained from the raw spectra; Bottom panel: experimentally obtained spectra for oxyferrous DHP B reacted with 2,4dibromophenol (black, t = 0 s), its reduction to the ferric enzyme (red, t = 11.6 s) and last species (blue, t = 49s). B) 2.6-dibromophenol: Top panel: stopped-flow UV-visible spectra of the single-mixing reacting of oxyferrous WT DHP B (10  $\mu$ M) preincubated with 10 equiv. of 2,6-dibromophenol and reacted with 10 equiv. of H<sub>2</sub>O<sub>2</sub> (900 scans over 49 s); inset: the single wavelength (419 nm) dependence on time obtained from the raw spectra; Bottom panel: experimentally obtained spectra for oxyferrous DHP B reacted with 2,6-dibromophenol (black, t = 0s), its reduction to the ferric enzyme (red, t = 12.9 s) and last species (blue, t = 49 s). (For interpretation of the references to colour in this figure

legend, the reader is referred to the web version of this article.)

to 6. A more thorough examination of the monomeric oxidation products for 2,4-DCP and 2,4-DBP showed two different oxidation pathways for both substrates, namely oxidation (Scheme 1, pathway A) and oxidative dehalogenation (Scheme 2, pathway B). Thus, to determine the origin of the oxygen atom(s) incorporated into the substrates upon product formation, isotopic labeling studies with <sup>18</sup>O were performed. For both oxidation pathways, the first oxygen atom incorporated into the initial diol product was derived exclusively from water and the second oxygen atom incorporated into the diol product derived exclusively from hydrogen peroxide, providing unequivocal evidence of peroxidase and peroxygenase activities, respectively. The sequential oxidation of dihalophenols, initially via a peroxidase pathway, followed by peroxygenase activity, and with further possible oxidation via peroxidase chemistry (in select cases), highlights the ability of these substrates to be converted into products by the multifunctional nature of DHP B. These mechanistic observations made for 2,4-DCP and 2,4-DBP likely apply to the other dihalophenols studied here, since similar monomeric products were observed for all substrates.

Interestingly, sequential and/or concomitant oxidative activities by DHP have been observed previously for 4-nitrophenol (4-NP) [41], 4-Xo-cresols [42] and 5-Br-indole [40]. In the case of 4-NP, the oxidation chemistry is opposite from that observed for DXP: the first inserted oxygen atom originates from hydrogen peroxide forming 4-nitrocatechol (4-NC), into which a second oxygen, derived from water, is added yielding a triol product, constituting sequential peroxygenase followed by peroxidase activities, respectively. Furthermore, the triol product is further oxidized to a quinone product via electron transfer (peroxidase activity) [41]. For 4-X-o-cresol substrates, non-preferential oxidation via either peroxidase or peroxygenase activities was observed, yielding quinone and catechol products, respectively [42]. And lastly, the DHPcatalyzed oxidation of 5-Br-indole yields oxindoles as the major products of a peroxygenase activity, which themselves undergo dimerization in the presence of molecular oxygen to form 5,5'-Br2-indigo via an oxidase activity [40]. The chemistry observed here for dihalophenols further highlights both the substrate and mechanistic promiscuity of dehaloperoxidase as a multifunctional catalytic globin.

Binding studies confirmed the affinities of the 2,4-DXP substrates in the order DBP > DCP > DFP, which is in accordance with the literature for other halogenated substrates whose affinities correlate with halogen size [42,46,49,40]. X-ray crystallographic studies on DHP complexed with 2,4-DCP and 2,4-DBP show these substrates are positioned inside the enzyme active site: two conformations were observed for 2,4-DCP ( $\alpha$ and  $\beta$ , Fig. 3C), with 2,4-DCP $_{\alpha}$  and 2,4-DBP having nearly identical positions in the substrate binding pocket (Fig. S15B). For both 2,4-DXP substrates (except 2,4-DCP<sub>B</sub>), the phenolic ring interacts with F21 via  $\pi$ - $\pi$  stacking interactions, and the hydroxyl group interacts with the distal histidine (H55, "closed" conformation) via H-bonding interaction. Moreover, the bulky p-halogen is well positioned in the Xe1 binding cavity region [49], consistent with other halogenated substrates 4-bromophenol [49], 2,4,6-tribromophenol [38], 5-bromoindole [40], 4bromo-o-guaiacol [46] and 4-bromo-o-cresol [42], resulting in displacement of F60. These strong interactions provide the molecular basis as to why 2,4-DBP and 2,4-DCP possess the smallest K<sub>d</sub> values for any DHP substrate (or ligand) reported to date. Recently, the structure of DHP B complexed with 2,4-DCP was elucidated by serial femtosecond Xray crystallography (SFX) [44], which confirmed the position of 2,4-DCP in the pocket, although only one conformation (2,4-DCP<sub>\alpha</sub>) was observed (Fig. S15A), likely a result of the different crystallization conditions employed between the two studies. Whether or not the two different conformations of 2,4-DCP ( $\alpha$  and  $\beta$ ) affect product distribution or oxidation pathway is unknown at this time.

The 2,6-DXP series shows a comparatively lower affinity for the enzyme in the order DFP > DCP > DBP, the opposite of what was observed for the 2,4-DXP series, and thus in contrast with literature reports as well. To rationalize this, the structures of DHP complexed with the 2,6-DXP series (X = F, Cl, Br) (Fig. S16) were elucidated, and

show interesting results. In these substrates, both halogens are vicinal to the hydroxyl group, and therefore positioned close together on one side of the ring. This substitution pattern on the phenolic ring seems to favor the binding of the substrate closer to the highly polar  $\gamma$  edge of the heme, where the substrate is in close proximity of the heme propionates and functionally important residues, such as H55 ("open" conformation) and Y38. The structure for 2,6-DCP and 2,6-DBP showed these two substrates binding in similar positions close to the entrance of the pocket, and interacting with hydrophilic amino acids T56 and Y38. The superimposed structure of 2,6-DCP and 2,4,6-TCP<sub>ext</sub> showed similar substrate positions, although the hydroxyl group of 2,6-DCP is rotated internally by about  $\sim \! 35^{\circ}$ . In addition, DHP was found to have a very small affinity for 2,6-DBP ( $K_d \sim 7100 \,\mu\text{M}$ ), which correlated to the fact that it was only found to bind in protomer B (the absence of substrate in protomer A resulted in bis-histidine ligation) [46,47]. In a departure from the literature where 4-fluorophenol [49] and 4-fluoro-o-cresol [42] were found to bind closer to the entrance of the active site (and thus exhibit low affinities with DHP), 2,6-DFP binds internally in the same position occupied by 2,4-DCP $_{\alpha}$  and 2,4-DBP, possibly due to the smaller size of the fluorine atoms. Overall, the absence of the p-halogen atom in 2,6-DXP has three main effects: i) a reverse order of binding affinity when compared to the 2,4-DXP series, ii) halogen atoms are interacting with polar residues (T56, H55 and Y38F), and iii) a reverse of the traditional binding positions in the hydrophobic cavity of DHP. Nonetheless, these structural differences in binding position do not translate into an activity loss, and in fact, a near 100% substrate conversion was observed in the oxidation reactions of the 2,6-DXP series despite employing nonoptimized conditions.

A structural comparison of the mono- (4-XP), di- (2,4-DXP) and trihalophenol (2,4,6-TXP) substrates further reveals insights into the structure-function relationship of DHP (Fig. S15), with the three brominated halophenol derivatives occupying distinct positions in the active site pocket: i) 4-BP is close to the pocket entrance, perpendicular to the heme plane, interacting with Y38 and propionate D, and forcing H55 to a "open" conformation (solvent exposed); ii) 2,4-DBP is positioned internally with the OH group 4.9 Å away from the iron center, interacting with F21 and H55 in the closed conformation; and iii) 2,4,6-TBP is also positioned internally, although rotated slightly when compared to 2,4-DBP (p-Br groups are separated by 3.9 Å), with the OH group directed towards the iron center (3.9 Å). The comparison between the mono-, di-, and trichlorophenols is more complex because both 2,4-DCP ( $\alpha$  and  $\beta$ ) and 2,4,6-TCP (int and ext) show two different binding positions in the pocket. For clarity, 2,4-DCP $_{\alpha}$  will be compared to 2,4,6-TCP<sub>int</sub>, and 2,4-DCP<sub>B</sub> will be compared to 2,4,6-TCP<sub>ext</sub>. The position observed for i) 4-CP is nearly identical to 4-BP; ii) 2,4-DCP $_{\alpha}$  and 2,4,6-TCP<sub>int</sub> are both positioned internally with similar orientations, with the o-Cl and OH groups almost overlapping (<1 Å apart), but the p-Cl groups are 3.2 Å apart; and iii) 2,4-DCP<sub>β</sub> and 2,4,6-TCP<sub>ext</sub> show similar positions to 4-CP, perpendicular to the heme plane, and close to the pocket entrance in the order: 2,4,6-TCP<sub>ext</sub>, 4-CP and 2,4-DCP<sub>β</sub>, as reflected by the distance between their hydroxyl group and propionate D (2.4, 3.2 and 4.8 Å, respectively).

A similar structural comparison of the 2,6-DXP series with mono- (4-XP) and trihalophenols (2,4,6-TXP) also reveals important insights. For the 2,6-DXP series, the absence of the *p*-halogen translates into low affinity resulting from a more solvent exposed binding position (except for 2,6-DFP). Adding a third halogen reduces favorable F21 interactions through molecular rotation, as the trihalogenated substrate binds deeper to accommodate the additional steric bulk, which severs the H55 interactions. Removing one halogen atom makes 4-XP more polar compared to their DXP counterparts, reflected in their position closer to the entrance of the pocket (more solvent exposed), where the interactions between F21 and H55 are replaced by new H-bonding interactions between the substrate OH group and Y38 and propionate D. Thus, by analyzing the stabilization factors surrounding each binding site, it is clear that the extremely tight binding affinity of DHP B for 2,4-

 $DCP_{\alpha}$  and 2,4-DBP is supported by favorable interactions and binding orientations, namely: the presence of two halogen atoms in 2,4-DXP places the phenol into an orientation that favors  $\pi$ – $\pi$  stacking interactions with F21, the o-halogen into the well-established Xe1 site, the p-halogen deep into the hydrophobic cavity, displacing residue F60, and further stabilization where OH—H55 interact via H-bonding.

As the principal reactive species in heme peroxidases [15,77–79], P450s [80-84], peroxygenases [84-89] and other hemoproteins [89-94], the ferryl-containing Compound I, ES, and II intermediates were explored here for their mechanistic roles in the DHP B-catalyzed oxidation of DXP substrates. Overall, the results show that all three activated forms of DHP are catalytically competent species in the oxidation of DXP substrates, themselves being reduced to the ferric resting state. The mechanistic studies performed with the brominated substrates showed the rate of reduction to ferric DHP B followed the order: Compound I > Compound II > Compound ES, which differs from previous studies where Compound ES was more rapidly reduced by substrates when compared to Compound II [11,41,42,45,46,40]. Additionally, the rate of Compound ES reduction by both 2,4 and 2,6-DXP followed the order: Br > Cl > F, where the brominated derivatives reacted faster than their fluorinated counterparts, similar to the 4-X-ocresol substrate series [42]. The DXP substrates were also found to activate the oxyferrous enzyme in the presence of H<sub>2</sub>O<sub>2</sub>, albeit without the formation of an intermediate, i.e. Compound II, whose transient formation was seen for halophenols [12], haloindoles [40], nitrophenol [41], and pyrroles [45], but not for guaiacols [46], and cresols [42]. The ability for DXP to enable DHP activation is critical, as the oxyferrous enzyme (hemoglobin-active) is normally unreactive towards H2O2 (in the absence of a substrate), which is likely a defense mechanism against autooxidation [17,12].

Of note, however, is that oxyferrous DHP was never observed as the final oxidation state when employing Compounds I, ES, or II to oxidize the DXP, even at longer reaction times, and is a departure from the product-driven aerobic reduction of the enzyme [20,46,40] that has been a hallmark of DHP reactivity as a multifunctional catalytic hemoglobin, one that provides a link between its enzymatic activities and its  $O_2$ -carrier function. We surmise that the competing oxidation pathways when starting with ferryl DHP leads to multiple products that do not produce a sufficient concentration of a reducing product, previously (and counterintuitively) identified as quinones [20,42,46] or oxindoles

[40], such that the further product-driven reduction to oxyferrous DHP is not observed. This product-driven reduction is likely an important mechanism used by the enzyme to rescue the hemoglobin-active form after catalytic activity initially renders DHP incapable of binding dioxygen in the enzymatic resting ferric state [9,17,18,50]. Although the product-driven reduction of ferric DHP B was not observed when starting with the ferryl species (Compounds I, ES and II), it was gratifying to observe DHP return to the oxyferrous form when enzymatic activity was initiated from this same oxyferrous state, suggesting that dihalophenols are likely physiologically-relevant given that the product-driven reduction of DHP occurs for physiological substrates (i.e., trihalophenols [5,9,12,17,20,50], haloindoles [40] and guaiacols [46]).

On the basis of the results obtained above, we propose the following catalytic cycle for the in vitro H<sub>2</sub>O<sub>2</sub>-dependent oxidation of 2,4-dibromophenol (2,4-DBP) as a representative substrate (Scheme 3): ferric DHP B reacts with 1 equiv. H<sub>2</sub>O<sub>2</sub> forming Compound I, a two-electron oxidized ferryl species [Por + Fe N = O AA] (step i), which undergoes fast internal electron transfer in DHP, yielding Compound ES [Por Fe<sup>IV</sup>=O •Tyr38]. Compound I can be reduced by 2,4-DBP (step ii) in a two-electron process given the lack of an observable intermediate, while Compound ES can be reduced by two sequential one-electron steps [8,23], first leading to formation of Compound II [Por Fe<sup>IV</sup>=O AA] (step iii) before further reduction to the resting ferric enzyme (step iv). The ferric enzyme is then available for reactivation by a second equivalent of hydrogen peroxide, which could lead to the formation of products through a peroxidase mechanism via either pathway A (oxidation product 1a) or B (oxidative dehalogenation - product 1d). When pathway A occurs, a second oxygen is inserted via a peroxygenase mechanism (product 1b), followed by electron transfer through another peroxidase mechanism (product 1c). Compound II, formed by the reaction of oxyferrous DHP B with DXP and H2O2 (step v), can be reduced to the ferric enzyme by 2,4-DBP (step iv). While we did not observe Compound II when employing 2,4-DCP as a substrate when starting from oxyferrous DHP B (step v). It is likely that when starting from the oxyferrous form, Compound II is formed initially, and the catalytic cycle commences directly from Compound II and proceeds as stated in Scheme 3. Alternatively, it has been demonstrated both here with 2,4-DBP and previously with other substrates that DHP B is able to initiate both peroxidase and peroxygenase catalytic cycles [20,41,42,45,46,40,76] through H<sub>2</sub>O<sub>2</sub>-activation of the globin-active oxyferrous state yielding

NH. AA 
$$H_2O_2$$
 (i)  $H_2O$  (ii)  $H_2O$  (iii)  $H_2O$  (iv)  $H_2O_2$  (iv)  $H_2O$  (iv)  $H_2O_2$  (iv)  $H$ 

Scheme 3. Proposed mechanism for the DHP B-catalyzed sequential oxidation of 2,4-DBP as a representative DXP substrate.

the ferric enzyme (step vi), with product-driven reduction capable of rescuing the  $O_2$ -transport function of DHP (step vii) should such quinone products be produced in sufficient quantity. We note that oxyferrous DHP was observed as the final 'resting' state of the enzyme when the catalytic cycle was initiated from this same oxyferrous state.

### 5. Conclusion

In summary, DHP B reactivity studies with 2,4- and 2,6-dihalophenols (DXP) confirm this multifunctional catalytic globin is capable of oxidizing these substrates under physiological conditions. Product identification coupled with isotopic labeling shows two simultaneous pathways in the oxyfunctionalization of these substrates, namely oxidation and oxidative dehalogenation. In both pathways, the initial substrate oxidation occurs through a peroxidase activity, with further subsequent oxidation proceeding via a peroxygenase mechanism. X-ray crystallographic studies enabled comparison of the DXP substrates to both the monohalogenated (4-XP) and trihalogenated (2,4,6-TXP) analogs: 2,4-DCP $_{\alpha}$  and 2,4-DBP bind in a similar orientation as 2,4,6-TXP $_{int}$ , and 2.4-DCP<sub>8</sub> and 2.6-DCP were found in similar positions as 2.4.6-TCP<sub>evt</sub>, providing a possible explanation for the two oxvfunctionalization pathways based on substrate binding/orientation in the DHP active site. The inhibitory function of 4-halophenols can be explained by their more unique position in the pocket, virtually blocking the entrance of any other molecules, which prevents binding of other substrates or H<sub>2</sub>O<sub>2</sub> activation (by hindering the distal histidine from serving as the general acid/base in the 'closed' conformation) [30,32,35,49,52]. Thus, as structural intermediaries between the 4-XP (inhibitors) and 2,4,6-TXP (peroxidase substrates), the results presented here on 2,4-DXP once again highlight the unexpected and unpredictable chemistry of DHP as a multifunctional catalytic globin, namely how a hemoglobin active site that enables multiple substrate binding conformations also enables the substrate itself to influence the different catalytic mechanisms that DHP B performs on it, either exclusively, simultaneously or sequentially, that lead to product formation.

### Author statement

Talita Malewschik, Leah Carey and Vesna de Serrano were responsible for data curation, investigation, methodology and writing - original draft; Reza A. Ghiladi was responsible for conceptualization, funding acquisition, project administration, and writing - review & editing.

# **Declaration of Competing Interest**

The authors declare that they have no known competing financial interests or personal relationships that could have appeared to influence the work reported in this paper.

# Data availability

Data will be made available on request.

# Acknowledgements

This project was supported by the National Science Foundation (CHE-1609446 and CHE-2002954). This work was performed in part by the Molecular Education, Technology and Research Innovation Center (METRIC) at NC State University, which is supported by the State of North Carolina. X-ray diffraction data were collected at Southeast Regional Collaborative Access Team (SER-CAT) ID22 and BM22 beamlines at the Advanced Photon Source, Argonne National Laboratory. Supporting institutions may be found at <a href="https://www.ser-cat.org/">www.ser-cat.org/</a> members. html. Use of the Advanced Photon Source was supported by the U. S. Department of Energy, Office of Science, Office of Basic Energy Sciences,

under Contract No. W-31-109-Eng-38.

# Appendix A. Supplementary data

Supplementary data to this article can be found online at https://doi.org/10.1016/j.jinorgbio.2022.111944.

### References

- J.W. Scott, Some egg-laying habits of Amphitrite ornata verrill, Biol. Bull. 17 (1909) 327–340
- [2] G.W. Gribble, The diversity of naturally produced organohalogens, Chemosphere 52 (2003) 289–297, https://doi.org/10.1016/S0045-6535(03)00207-8.
- [3] G.W. Gribble, Naturally Occurring Organohalogen Compounds A Comprehensive Update, Springer-Verlag Vienna, 2010.
- [4] D.E. Lincoln, K.T. Fielman, R.L. Marinelli, S.A. Woodin, Bromophenol accumulation and sediment contamination by the marine annelids *Notomastus lobatus* and *Thelepus crispus*, Biochem. Syst. Ecol. 33 (2005) 559–570, https://doi. org/10.1016/j.bse.2004.12.006.
- [5] Y.P. Chen, S.A. Woodin, D.E. Lincoln, C.R. Lovell, An unusual dehalogenating peroxidase from the marine terebellid polychaete *Amphitrite ornata*, J. Biol. Chem. 271 (1996) 4609–4612, https://doi.org/10.1074/jbc.271.9.4609.
- [6] R.E. Weber, C. Mangum, H. Steinman, C. Bonaventura, B. Sullivan, J. Bonaventura, Hemoglobins of two terebellid polychaetes: *Enoplobranchus sanguineus* and *Amphitrite ornata*, Comp. Biochem. Physiol. Part A Physiol. 56 (1977) 179–187, https://doi.org/10.1016/0300-9629(77)90182-7.
- [7] L. Lebioda, M.W. LaCount, E. Zhang, Y.P. Chen, K. Han, M.M. Whitton, D. E. Lincoln, S.A. Woodin, An enzymatic globin from a marine worm, Nature. 401 (1999) 445, https://doi.org/10.1038/46728.
- [8] S. Franzen, R.A. Ghiladi, L. Lebioda, J. Dawson, Chapter 10: multi-functional hemoglobin dehaloperoxidases, RSC Met. (2016) 218–244, https://doi.org/ 10.1039/9781782622628-00218.
- [9] S. Sun, M. Sono, J. Du, J.H. Dawson, Evidence of the direct involvement of the substrate tcp radical in functional switching from oxyferrous O2 carrier to ferric peroxidase in the dual-function hemoglobin/dehaloperoxidase from *Amphitrite* ornata, Biochemistry 53 (2014) 4956–4969, https://doi.org/10.1021/bi5002757.
- [10] R. Davydov, R.L. Osborne, M. Shanmugam, J. Du, J.H. Dawson, B.M. Hoffman, Probing the oxyferrous and catalytically active ferryl states of *Amphitrite ornata* dehaloperoxidase by cryoreduction and EPR/ENDOR spectroscopy. Detection of compound I, J. Am. Chem. Soc. 132 (2010) 14995–15004, https://doi.org/ 10.1021/ja1059747.
- [11] R. Dumarieh, J. D'Antonio, A. Deliz-Liang, T. Smirnova, D.A. Svistunenko, R. A. Ghiladi, Tyrosyl radicals in dehaloperoxidase: how nature deals with evolving an oxygen-binding globin to a biologically relevant peroxidase, J. Biol. Chem. 288 (2013) 33470–33482, https://doi.org/10.1074/jbc.M113.496497.
- [12] J. D'Antonio, R.A. Ghiladi, Reactivity of deoxy- and oxyferrous dehaloperoxidase B from Amphinrite ornata: identification of compound II and its ferrous-hydroperoxide precursor, Biochemistry. 50 (2011) 5999–6011, https://doi.org/10.1021/bi200311u |.
- [13] J. Feducia, R. Dumarieh, L.B. Gilvey, T. Smirnova, S. Franzen, R.A. Ghiladi, Characterization of dehaloperoxidase compound ES and its reactivity with trihalophenols, Biochemistry 48 (2009) 995–1005, https://doi.org/10.1021/ bi801916i.
- [14] M.K. Thompson, S. Franzen, R.A. Ghiladi, B.J. Reeder, D.A. Svistunenko, Compound ES of dehaloperoxidase decays via two alternative pathways depending on the conformation of the distal histidine, J. Am. Chem. Soc. 132 (2010) 17501–17510, https://doi.org/10.1021/ja106620q.
- [15] R. Davydov, R.L. Osborne, H.K. Sun, J.H. Dawson, B.M. Hoffman, EPR and ENDOR studies of cryoreduced compounds II of peroxidases and myoglobin. Protoncoupled electron transfer and protonation status of ferryl hemes, Biochemistry 47 (2008) 5147–5155, https://doi.org/10.1021/bi702514d.
- [16] T.I. Smirnova, R.T. Weber, M.F. Davis, S. Franzen, Substrate binding triggers a switch in the iron coordination in dehaloperoxidase from *Amphitrite ornata*: HYSCORE experiments, J. Am. Chem. Soc. 130 (2008) 2128–2129, https://doi. org/10.1021/ja0772952.
- [17] J. Du, M. Sono, J.H. Dawson, Functional switching of Amphitrite ornata dehaloperoxidase from O 2-binding globin to peroxidase enzyme facilitated by halophenol substrate and H2O2, Biochemistry 49 (2010) 6064–6069, https://doi.org/10.1021/bi100741z.
- [18] S. Franzen, M.K. Thompson, R.A. Ghiladi, The dehaloperoxidase paradox, Biochim. Biophys. Acta Protein Proteomics 2012 (1824) 578–588, https://doi.org/10.1016/j.bbapap.2011.12.008.
- [19] S. Franzen, L.B. Gilvey, J.L. Belyea, The pH dependence of the activity of dehaloperoxidase from *Amphitrite ornata*, Biochim. Biophys. Acta Protein Proteomics 1774 (2007) 121–130, https://doi.org/10.1016/j. bbapap.2006.09.019.
- [20] J. D'Antonio, E.L. D'Antonio, M.K. Thompson, E.F. Bowden, S. Franzen, T. Smirnova, R.A. Ghiladi, Spectroscopic and mechanistic investigations of dehaloperoxidase B from Amphitrite ornata, Biochemistry 49 (2010) 6600–6616, designation.
- [21] J. Belyea, L.B. Gilvey, M.F. Davis, M. Godek, T.L. Sit, S.A. Lommel, S. Franzen, Enzyme function of the globin dehaloperoxidase from *Amphitrite ornata* is activated

- by substrate binding, Biochemistry 44 (2005) 15637–15644, https://doi.org/
- [22] L. Szatkowski, M.K. Thompson, R. Kaminski, S. Franzen, A. Dybala-Defratyka, Oxidative dechlorination of halogenated phenols catalyzed by two distinct enzymes: horseradish peroxidase and dehaloperoxidase, Arch. Biochem. Biophys. 505 (2011) 22–32, https://doi.org/10.1016/j.abb.2010.09.018.
- [23] R.L. Osborne, M.K. Coggins, G.M. Raner, M. Walla, J.H. Dawson, The mechanism of oxidative halophenol dehalogenation by *Amphitrite ornata* dehaloperoxidase is initiated by H 2 O 2 binding and involves two consecutive one-electron steps: role of ferryl intermediates, Biochemistry 48 (2009) 4231–4238, https://doi.org/ 10.1021/bi900367e.
- [24] C. Wang, L.L. Lovelace, S. Sun, J.H. Dawson, L. Lebioda, Complexes of dual-function hemoglobin/dehaloperoxidase with substrate 2,4,6-trichlorophenol are inhibitory and indicate binding of halophenol to compound I, Biochemistry 52 (2013) 6203–6210, https://doi.org/10.1021/bi400627w.
- [25] M.F. Davis, H. Gracz, F.A.P. Vendeix, V. De Serrano, A. Somasundaram, S. M. Decatur, S. Franzen, Different modes of binding of mono-, di-, and trihalogenated phenols to the hemoglobin dehaloperoxidase from *Amphitrite ornata*, Biochemistry 48 (2009) 2164–2172, https://doi.org/10.1021/bi801568s.
- [26] R.L. Osborne, L.O. Taylor, K. Han, B. Ely, J.H. Dawson, Amphitrite ornata dehaloperoxidase: enhanced activity for the catalytically active globin using MCPBA, Biochem. Biophys. Res. Commun. 324 (2004) 1194–1198, https://doi. org/10.1016/j.bbrc.2004.09.174.
- [27] T.L. Poulos, J. Kraut, The stereochemistry of peroxidase catalysis, J. Biol. Chem. 255 (1980) 8199–8205.
- [28] J. D'Antonio, Mechanistic Investigations of the Oxyferrous and Ferric States of Dehaloperoxidase B from Amphitrite ornata, 2012. http://www.lib.ncsu.edu/re solver/1840.16/9617.
- [29] E.L. D'Antonio, J. D'Antonio, V. De Serrano, H. Gracz, M.K. Thompson, R. A. Ghiladi, E.F. Bowden, S. Franzen, Functional consequences of the creation of an Asp-His-Fe triad in a 3/3 globin, Biochemistry 50 (2011) 9664–9680, https://doi.org/10.1021/bi201368u.
- [30] M.F. Davis, B.G. Bobay, S. Franzen, Determination of separate inhibitor and substrate binding sites in the dehaloperoxidase-hemoglobin from *Amphitrite ornata*, Biochemistry 49 (2010) 1199–1206, https://doi.org/10.1021/bi9018576.
- [31] J. Zhao, M. Xue, D. Gudanis, H. Gracz, G.H. Findenegg, Z. Gdaniec, S. Franzen, Dynamics of dehaloperoxidase-hemoglobin a derived from NMR relaxation spectroscopy and molecular dynamics simulation, J. Inorg. Biochem. 181 (2018) 65–73, https://doi.org/10.1016/j.jinorgbio.2018.01.006.
- [32] A. Plummer, M.K. Thompson, S. Franzen, Role of polarity of the distal pocket in the control of inhibitor binding in dehaloperoxidase-hemoglobin, Biochemistry 52 (2013) 2218–2227, https://doi.org/10.1021/bi301509r.
- [33] J. Belyea, C.M. Belyea, S. Lappi, S. Franzen, Resonance raman study of ferric heme adducts of dehaloperoxidase from *Amphitrite ornata*, Biochemistry 45 (2006) 14275–14284, https://doi.org/10.1021/bi0609218.
- [34] F.P. Nicoletti, M.K. Thompson, B.D. Howes, S. Franzen, G. Smulevich, New insights into the role of distal histidine flexibility in ligand stabilization of dehaloperoxidase-hemoglobin from *Amphitrite ornata*, Biochemistry 49 (2010) 1903–1912. https://doi.org/10.1021/bi9020567.
- 1903–1912, https://doi.org/10.1021/bi9020567.
  [35] M.K. Thompson, M.F. Davis, V. de Serrano, F.P. Nicoletti, B.D. Howes, G. Smulevich, S. Franzen, Internal binding of halogenated phenols in dehaloperoxidase-hemoglobin inhibits peroxidase function, Biophys. J. 99 (2010) 1586–1595, https://doi.org/10.1016/j.bpi.2010.05.041
- 1586–1595, https://doi.org/10.1016/j.bpj.2010.05.041.
  [36] J. Zhao, J. Moretto, P. Le, S. Franzen, Measurement of internal substrate binding in dehaloperoxidase-hemoglobin by competition with the heme-fluoride binding equilibrium, J. Phys. Chem. B 119 (2015) 2827–2838, https://doi.org/10.1021/ips12006v
- [37] R.L. Osborne, S. Sumithran, M.K. Coggins, Y.P. Chen, D.E. Lincoln, J.H. Dawson, Spectroscopic characterization of the ferric states of *Amphitrite ornata* dehaloperoxidase and *Notomastus lobatus* chloroperoxidase: His-ligated peroxidases with globin-like proximal and distal properties, J. Inorg. Biochem. 100 (2006) 1100–1108, https://doi.org/10.1016/j.jinorgbio.2006.02.008.
  [38] J. Zhao, V. De Serrano, J. Zhao, P. Le, S. Franzen, Structural and kinetic study of an
- [38] J. Zhao, V. De Serrano, J. Zhao, P. Le, S. Franzen, Structural and kinetic study of an internal substrate binding site in dehaloperoxidase-hemoglobin a from *Amphitrite* ornata, Biochemistry 52 (2013) 2427–2439, https://doi.org/10.1021/bi301307f.
- [39] M.W. LaCount, E. Zhang, Y.P. Chen, K. Han, M.M. Whitton, D.E. Lincoln, S. A. Woodin, L. Lebioda, The crystal structure and amino acid sequence of dehaloperoxidase from *Amphitrite ornata* indicate common ancestry with globins, J. Biol. Chem. 275 (2000) 18712–18716, https://doi.org/10.1074/jbc.M001194200.
- [40] D.A. Barrios, J. D'Antonio, N.L. McCombs, J. Zhao, S. Franzen, A.C. Schmidt, L. A. Sombers, R.A. Ghiladi, Peroxygenase and oxidase activities of dehaloperoxidase-hemoglobin from *Amphitrite ornata*, J. Am. Chem. Soc. 136 (2014) 7914–7925, https://doi.org/10.1021/ja500293c.
- [41] N.L. McCombs, J. D'Antonio, D.A. Barrios, L.M. Carey, R.A. Ghiladi, Nonmicrobial nitrophenol degradation via peroxygenase activity of dehaloperoxidasehemoglobin from *Amphitrite ornata*, Biochemistry 55 (2016) 2465–2478, https:// doi.org/10.1021/acs.biochem.6b00143.
- [42] T. Malewschik, V. de Serrano, A.H. McGuire, R.A. Ghiladi, The multifunctional globin dehaloperoxidase strikes again: simultaneous peroxidase and peroxygenase mechanisms in the oxidation of EPA pollutants, Arch. Biochem. Biophys. 673 (2019), 108079, https://doi.org/10.1016/j.abb.2019.108079.
- [43] N.L. McCombs, Unraveling the Multiple Enzymatic Activities of the Dehaloperoxidase-Hemoglobin From Amphitrite ornata, 2017.
- [44] T. Moreno-Chicano, A. Ebrahim, D. Axford, M.V. Appleby, J.H. Beale, A.K. Chaplin, H.M.E. Duyvesteyn, R.A. Ghiladi, S. Owada, D.A. Sherrell, R.W. Strange,

- H. Sugimoto, K. Tono, J.A.R. Worrall, R.L. Owen, M.A. Hough, High-throughput structures of protein-ligand complexes at room temperature using serial femtosecond crystallography, IUCrJ. 6 (2019) 1074–1085, https://doi.org/10.1107/S205225519011655.
- [45] N.L. McCombs, T. Smirnova, R.A. Ghiladi, Oxidation of pyrrole by dehaloperoxidase-hemoglobin: chemoenzymatic synthesis of pyrrolin-2-ones, Catal, Sci. Technol. 7 (2017) 3104–3118, https://doi.org/10.1039/c7cy00781g
- [46] A.H. Mcguire, L.M. Carey, V. De Serrano, S. Dali, R.A. Ghiladi, L.M. Carey, V. De Serrano, S. Dali, R.A. Ghiladi, Leroxidase versus peroxygenase activity: substrate substituent effects as modulators of enzyme function in the multifunctional catalytic globin dehaloperoxidase, Biochemistry 57 (2018) 4455–4468, https://doi.org/10.1021/acs.biochem.8b00540.
- [47] N.L. McCombs, T. Moreno-Chicano, L.M. Carey, S. Franzen, M.A. Hough, R. A. Ghiladi, Interaction of azole-based environmental pollutants with the coelomic hemoglobin from *Amphitrite ornata*: a molecular basis for toxicity, Biochemistry 56 (2017) 2294–2303, https://doi.org/10.1021/acs.biochem.7b00041.
- [48] J. Zhao, S. Franzen, Kinetic study of the inhibition mechanism of dehaloperoxidase-hemoglobin a by 4-bromophenol, J. Phys. Chem. B 117 (2013) 8301–8309, https://doi.org/10.1021/jp3116353.
- [49] V. De Serrano, S. Franzen, Structural evidence for stabilization of inhibitor binding by a protein cavity in the dehaloperoxidase-hemoglobin from *Amphitrite ornata*, Biopolym, Pept. Sci. 98 (2011) 27–35, https://doi.org/10.1002/bip.21674.
- [50] S. Sun, M. Sono, C. Wang, J. Du, L. Lebioda, J.H. Dawson, Influence of heme environment structure on dioxygen affinity for the dual function *Amphitrite ornata* hemoglobin/dehaloperoxidase. Insights into the evolutional structure-function adaptations, Arch. Biochem. Biophys. 545 (2014) 108–115, https://doi.org/ 10.1016/j.abb.2014.01.010.
- [51] S. Jiang, I. Wright, P. Swartz, S. Franzen, The role of T56 in controlling the flexibility of the distal histidine in dehaloperoxidase-hemoglobin from *Amphitrite* ornata, Biochim. Biophys. Acta Protein Proteomics 2013 (1834) 2020–2029, https://doi.org/10.1016/j.bbapap.2013.06.005.
- [52] Z. Zhang, A.P. Santos, Q. Zhou, L. Liang, Q. Wang, T. Wu, S. Franzen, Steered molecular dynamics study of inhibitor binding in the internal binding site in dehaloperoxidase-hemoglobin, Biophys. Chem. 211 (2016) 28–38, https://doi.org/ 10.1016/j.bpc.2016.01.003.
- [53] Z. Chen, V. De Serrano, L. Betts, S. Franzen, Distal histidine conformational flexibility in dehaloperoxidase from *Amphitrite ornata*, Acta Crystallogr. Sect. D Biol. Crystallogr. 65 (2009) 34–40, https://doi.org/10.1107/ S0907444908036548.
- [54] J. Zhao, V. de Serrano, R. Dumarieh, M. Thompson, R.A. Ghiladi, S. Franzen, The role of the distal histidine in H2O2 activation and heme protection in both peroxidase and globin functions, J. Phys. Chem. B 116 (2012) 12065–12077, https://doi.org/10.1021/jp300014b.
  [55] K. Han, S.A. Woodin, D.E. Lincoln, K.T. Fielman, B. Ely, Amphitrite ornata, a marine
- [55] K. Han, S.A. Woodin, D.E. Lincoln, K.T. Fielman, B. Ely, Amphitrite ornata, a marine worm, contains two dehaloperoxidase genes, Mar. Biotechnol. 3 (2001) 287–292, https://doi.org/10.1007/s10126-001-0003-8.
- [56] L.M. Carey, R. Gavenko, D.A. Svistunenko, R.A. Ghiladi, How nature tunes isoenzyme activity in the multifunctional catalytic globin dehaloperoxidase from *Amphitrite ornata*, Biochim. Biophys. Acta Protein Proteomics 2018 (1866) 230–241, https://doi.org/10.1016/j.bbapap.2017.11.004.
- [57] A. Castro-Forero, D. Jimenez, J. Lopez-Garriga, M. Torres-Lugo, Immobilization of myoglobin from horse skeletal muscle in hydrophobic polymer networks, J. Appl. Polym. Sci. 107 (2008) 881–890, https://doi.org/10.1002/app.
- [58] N.V. Goral, D.A. Ryabov, Reactivity of the horseradish peroxidase compounds I and II toward organometallic substrates, Biochem. Mol. Biol. Int. 45 (1998) 61–71.
- [59] R.F. Beers, I.W. Sizer, A spectroscopic method for measuring the breakdown of hydrogen peroxide by catalase, J. Biol. Chem. 195 (1952) 133–140.
- [60] P. Chenprakhon, J. Sucharitakul, B. Panijpan, P. Chaiyen, Measuring binding affinity of protein-ligand interaction using spectrophotometry: binding of neutral red to riboflavin-binding protein, J. Chem. Educ. 87 (2010) 829–831, https://doi. org/10.1021/ed1000125.
- [61] Z. Otwinoswski, W. Minor, Processing of X-ray diffraction data collected in oscillation mode, Methods Enzymol. 276 (1997) 307–326, https://doi.org/ 10.1016/S0076-6879(97)76066-X.
- [62] A.J. McCoy, R.W. Grosse-Kunstleve, P.D. Adams, M.D. Winn, L.C. Storoni, R. J. Read, Phaser crystallographic software, J. Appl. Crystallogr. 40 (2007) 658–674, https://doi.org/10.1107/S0021889807021206.
- [63] P.D. Adams, P.V. Afonine, G. Bunkóczi, V.B. Chen, I.W. Davis, N. Echols, J. J. Headd, L.W. Hung, G.J. Kapral, R.W. Grosse-Kunstleve, A.J. McCoy, N. W. Moriarty, R. Oeffner, R.J. Read, D.C. Richardson, J.S. Richardson, T. C. Terwilliger, P.H. Zwart, PHENIX: a comprehensive Python-based system for macromolecular structure solution, Acta Crystallogr. Sect. D Biol. Crystallogr. D66 (2010) 213–221, https://doi.org/10.1107/S0907444909052925.
- [64] V. de Serrano, J. D'Antonio, S. Franzen, R.A. Ghiladi, S.A. Woodin, J.H. Dawson, L. Lebioda, Structure of dehaloperoxidase B at 1.58 Å resolution and structural characterization of the AB dimer from Amphitrite ornata, Acta Crystallogr. Sect. D Biol. Crystallogr. 66 (2010) 529–538, https://doi.org/10.1107/ S0007444010004580
- [65] P. Emsley, B. Lohkamp, W.G. Scott, K. Cowtan, Features and development of Coot, Acta Crystallogr. Sect. D Biol. Crystallogr. D66 (2010) 486–501, https://doi.org/ 10.1107/S0907444910007493.
- [66] P.V. Afonine, R.W. Grosse-Kunstleve, N. Echols, J.J. Headd, N.W. Moriarty, M. Mustyakimov, T.C. Terwilliger, A. Urzhumtsev, P.H. Zwart, P.D. Adams, Towards automated crystallographic structure refinement with phenix.refine, Acta Crystallogr. Sect. D Biol. Crystallogr. D68 (2012) 352–367, https://doi.org/ 10.1107/S0907444912001308.

- [67] G.N. Murshudov, A.A. Vagin, E.J. Dodson, Refinement of macromolecular structures by the maximum-likelihood method, Acta Crystallogr. Sect. D Biol. Crystallogr. 53 (1997) 240–255, https://doi.org/10.1107/S0907444996012255.
- [68] C.C. Project, The CCP4 suite: programs for protein crystallography, Acta Crystallogr. Sect. D Biol. Crystallogr. 50 (1994) 760–763, https://doi.org/ 10.1107/S0907444994003112.
- [69] M. Yang, X. Zhang, Comparative developmental toxicity of new aromatic halogenated DBPs in a chlorinated saline sewage effluent to the marine *Polychaete* platynereis dumerilii, Environ. Sci. Technol. 47 (2013) 10868–10876, https://doi. org/10.1021/es401841t.
- [70] A.H. McGuire, When a hemoglobin acts as a catalytic enzyme, in: Mechanistic Studies of Dehaloperoxidase, 2020.
- [71] J.H. Gross, Mass Spectrometry: A Textbook, 3rd ed., 2017.
- [72] S. Franzen, K. Sasan, B.E. Sturgeon, B.J. Lyon, B.J. Battenburg, H. Gracz, R. Dumarieh, R.A. Ghiladi, Nonphotochemical base-catalyzed hydroxylation of 2,6dichloroquinone by H2O2 occurs by a radical mechanism, J. Phys. Chem. B 116 (2012) 1666–1676, https://doi.org/10.1021/jp208536x.
- [73] L.M. Carey, K.B. Kim, N.L. Mccombs, P. Swartz, C. Kim, R.A. Ghiladi, Selective tuning of activity in a multifunctional enzyme as revealed in the F21W mutant of dehaloperoxidase B from *Amphitrite ornata*, J. Biol. Inorg. Chem. 23 (2018) 209–219, https://doi.org/10.1007/s00775-017-1520-x.
- [74] P.A. Sigala, D.A. Kraut, J.M.M. Caaveiro, B. Pybus, E.A. Ruben, D. Ringe, G. A. Petsko, D. Herschlag, Testing geometrical discrimination within an enzyme active site: constrained hydrogen bonding in the ketosteroid isomerase oxyanion hole, J. Am. Chem. Soc. 130 (2008) 13696–13708, https://doi.org/10.1021/ia803928m
- [75] P. Auffinger, F.A. Hays, E. Westhof, P.S. Ho, Halogen bonds in biological molecules, Proc. Natl. Acad. Sci. U. S. A. 101 (2004) 16789–16794, https://doi. org/10.1073/pnas.0407607101.
- [76] D.A. Barrios, Probing the mechanism and reactivity of biomacromolecular and small molecule catalytic systems with H<sub>2</sub>O<sub>2</sub> and O<sub>2</sub>, 2013, https://doi.org/ 10.1038/46728. http://www.lib.ncsu.edu/resolver/1840.16/8864.
- [77] H.B. Dunford, Heme Peroxidases, Wiley-VCH, New York, 1999.
- [78] H.B. Dunford, J.S. Stillman, On the function and mechanism of action of peroxidases, Coord. Chem. Rev. 19 (1976) 187–251, https://doi.org/10.1016/ S0010-8545(00)80316-1.
- [79] T.L. Poulos, Thirty years of heme peroxidase structural biology, Arch. Biochem. Biophys. 500 (2010) 3–12, https://doi.org/10.1016/j.abb.2010.02.008.
- [80] M. Sono, M.P. Roach, E.D. Coulter, J.H. Dawson, Heme-containing oxygenases, Chem. Rev. 96 (1996) 2841–2888, https://doi.org/10.1021/cr9500500.

- [81] B. Meunier, S.P. de Visser, S. Shaik, Mechanism of oxidation reactions catalyzed by cytochrome P450 enzymes, Chem. Rev. 104 (2004) 3947–3980, https://doi.org/ 10.1021/cr020443g.
- [82] X. Huang, J.T. Groves, Oxygen activation and radical transformations in heme proteins and metalloporphyrins, Chem. Rev. 118 (2018) 2491–2553, https://doi. org/10.1021/acs.chemrev.7b00373.
- [83] X. Wang, S. Peter, R. Ullrich, M. Hofrichter, J.T. Groves, Driving force for oxygenatom transfer by heme-thiolate enzymes, Angew. Chem. Int. Ed. 52 (2013) 9238–9241, https://doi.org/10.1002/anie.201302137.
- [84] A.W. Munro, K.J. McLean, J.L. Grant, T.M. Makris, Structure and function of the cytochrome P450 peroxygenase enzymes, Biochem. Soc. Trans. 46 (2018) 183–196, https://doi.org/10.1042/BST20170218.
- [85] M. Faiza, S. Huang, D. Lan, Y. Wang, New insights on unspecific peroxygenases: superfamily reclassification and evolution, BMC Evol. Biol. 19 (2019) 1–19, https://doi.org/10.1186/s12862-019-1394-3.
- [86] C.E. Paul, E. Churakova, E. Maurits, M. Girhard, V.B. Urlacher, F. Hollmann, In situ formation of H2O2 for P450 peroxygenases, Bioorg. Med. Chem. 22 (2014) 5692–5696, https://doi.org/10.1016/j.bmc.2014.05.074.
- [87] O. Shoji, Y. Watanabe, Peroxygenase reactions catalyzed by cytochromes P450, J. Biol. Inorg. Chem. 19 (2014) 529–539, https://doi.org/10.1007/s00775-014-1106-9.
- [88] X. Wang, R. Ullrich, M. Hofrichter, J.T. Groves, Heme-thiolate ferryl of aromatic peroxygenase is basic and reactive, Proc. Natl. Acad. Sci. U. S. A. 112 (2015) 3686–3691, https://doi.org/10.1073/pnas.1503340112.
- [89] X. Wang, S. Peter, M. Kinne, M. Hofrichter, J.T. Groves, Detection and kinetic characterization of a highly reactive heme-thiolate peroxygenase compound i, J. Am. Chem. Soc. 134 (2012) 12897–12900, https://doi.org/10.1021/ja3049223
- [90] T. Matsui, S. Nagano, K. Ishimori, Y. Watanabe, I. Morishima, Preparation and reactions of myoglobin mutants bearing both proximal cysteine ligand and hydrophobic distal cavity: protein models for the active site of P-450, Biochemistry. 35 (1996) 13118–13124, https://doi.org/10.1021/bi960459z.
- [91] T. Matsui, S.I. Ozaki, Y. Watanabe, On the formation and reactivity of compound I of the His-64 myoglobin mutants, J. Biol. Chem. 272 (1997) 32735–32738, https://doi.org/10.1074/jbc.272.52.32735.
- [92] T.L. Poulos, Heme enzyme structure and function, Chem. Rev. 114 (2014) 3919–3962. https://doi.org/10.1021/cr400415k.
- [93] T. Matsui, S.I. Ozaki, E. Liong, G.N. Phillips, Y. Watanabe, Effects of the location of distal histidine in the reaction of myoglobin with hydrogen peroxide, J. Biol. Chem. 274 (1999) 2838–2844, https://doi.org/10.1074/jbc.274.5.2838.
- [94] M.T. Green, J.H. Dawson, H.B. Gray, Oxoiron(IV) in chloroperoxidase compound II is basic: Implications for P450 chemistry, Science 304 (80) (2004) 1653–1656, https://doi.org/10.1126/science.1096897.